JCI insight

Liver Sinusoidal Endothelial Cells Contribute to Portal Hypertension Through Collagen Type IV–Driven Sinusoidal Remodeling

Can Gan, … , Sheng Cao, Vijay H. Shah

JCI Insight. 2024. https://doi.org/10.1172/jci.insight.174775.

Research In-Press Preview Cell biology Hepatology

Graphical abstract

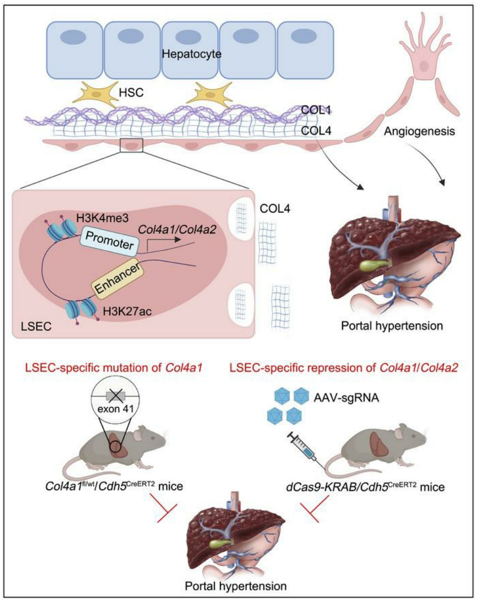

Liver Sinusoidal Endothelial Cells Contribute to Portal Hypertension Through Collagen Type IV–Driven Sinusoidal Remodeling

Can Gan, MBBS
Usman Yaqoob, MBBS
Jianwen Lu, MD
Man Xie, MD
Abid Anwar
Nidhi Jalan-Sakrikar, PhD
Sofia Jerez, PhD
Tejasav Sehrawat, MBBS
Amaia Navarro-Corcuera, PhD
Enis Kostallari, PhD, MS
Nawras W. Habash, MBBS
Sheng Cao, MD
Vijay H. Shah, MD

Author Affiliations: Department of Gastroenterology (Gan), West China Hospital, Sichuan University, China [Research Collaborator in the Division of Gastroenterology and Hepatology (limited tenure), Mayo Clinic, Rochester, Minnesota, USA]; Division of Gastroenterology and Hepatology (Yaqoob, Anwar, Jalan-Sakrikar, Kostallari, Cao, and Shah), Mayo Clinic, Rochester, Minnesota, USA; Research Fellow in the Division of Gastroenterology and Hepatology, Mayo Clinic, Rochester, Minnesota, and Department of Hepatobiliary Surgery, the First Affiliated Hospital of Xi'an Jiaotong University, Xi'an, Shaanxi, China (Lu), Research Fellow in the Division of Gastroenterology and Hepatology, Mayo Clinic, Rochester, Minnesota, and Department of Gastroenterology, Affiliated Hospital of Qingdao University, Qingdao, Shandong, China (Xie), Research Fellow in the

Division of Gastroenterology and Hepatology (Jerez, Sehrawat, and Navarro-Corcuera), and Resident in the Division of Gastroenterology and Hepatology , Mayo Clinic School of Graduate Medical Education, Mayo Clinic College of Medicine and Science, Rochester, Minnesota, USA.

Corresponding Authors: Vijay H. Shah, MD, Division of Gastroenterology and Hepatology, Mayo Clinic, 200 First St SW, Rochester, MN 55905 (shah.vijay@mayo.edu Phone: 507-255-6028 Fax: 507-255-6318); or Sheng Cao, MD, Division of Gastroenterology and Hepatology, Mayo Clinic, 200 First St SW, Rochester, MN 55905 (cao.sheng@mayo.edu Phone: 507-293-2385 Fax: 507-255-6318).

Conflict of interest: All authors have declared that no conflict of interest exists.

Text word count (all inclusive): 10,751
Abstract word count: 177
No. of tables: 0
No. of figures: 9
No. of supplemental tables: 2
No. of supplemental figures: 12
No. of supplemental videos: 1
Short title: LSEC-Derived COL4 Promotes PHTN

Abstract

Portal hypertension (PHTN) is a severe complication of liver cirrhosis and is associated with intrahepatic sinusoidal remodeling induced by sinusoidal resistance and angiogenesis. Collagen type IV (COL4), a major component of basement membrane, forms in liver sinusoids upon chronic liver injury. However, the role, the cellular source and expression regulation of COL4 in liver diseases is unknown. Here, we examined how COL4 is produced and how it regulates sinusoidal remodeling in fibrosis and PHTN. Human cirrhotic liver sample RNA-sequencing showed increased COL4 expression, which was further confirmed via immunofluorescence staining. scRNA-sequencing identified liver sinusoidal endothelial cells (LSECs) as the predominant source of COL4 upregulation in mouse fibrotic liver. In addition, COL4 was upregulated in a tumor necrosis factor α–nuclear factor–κB dependent manner through an epigenetic mechanism in liver sinusoidal endothelial cells *in vitro*. Indeed, by utilizing a CRISPRi-dCas9-KRAB-mediated epigenome editing approach, epigenetic repression of the enhancer-promoter interaction showed silencing of COL4 gene expression. LSEC-specific COL4 gene mutation or repression *in vivo* abrogated sinusoidal resistance and angiogenesis, which thereby alleviated sinusoidal remodeling and PHTN. Our findings reveal that LSECs promote sinusoidal remodeling and PHTN during liver fibrosis through COL4 deposition.

Keywords: liver sinusoidal endothelial cells; collagen type IV; portal hypertension; sinusoidal remodeling; enhancer-promoter interaction

Abbreviations:

AAV, adeno-associated virus

CCl_4, carbon tetrachloride

ChIP, chromatin immunoprecipitation

COL1, collagen type I

COL4, collagen type IV

CRISPRi-dCas9-KRAB, clustered regularly interspaced short palindromic repeat interference, inactive Cas9, Krüppel-associated box

ECM, extracellular matrix

ER, endoplasmic reticulum

FBS, fetal bovine serum

FITC, fluorescein isothiocyanate

H3K4me1, histone H3 methylation at lysine 4

H3K4me3, histone H3 trimethylation at lysine 4

H3K27ac, histone H3 acetylation at lysine 27

HSC, hepatic stellate cell

IF, immunofluorescence

IHC, immunohistochemical

LSEC, liver sinusoidal endothelial cell

NF-κB, nuclear factor–κB

PBS, phosphate-buffered saline

PHTN, portal hypertension

qPCR, quantitative real-time polymerase chain reaction

scRNA-Seq, single-cell RNA sequencing

sgRNA, single-guide RNA

siRNA, small interfering RNA

TAF-ChIP-Seq, tagmentation-assisted fragmentation of chromatin immunoprecipitation sequencing

TNFα, tumor necrosis factor-α

TGFβ, transforming growth factor-β

PDGFRβ: platelet-derived growth factor receptor-β

αSMA: α-smooth muscle actin

LYVE1: lymphatic vessel endothelial hyaluronan receptor 1

Introduction

Portal hypertension (PHTN) is a consequence of liver cirrhosis and a leading cause of liver transplant and death in patients with cirrhosis (1). According to the hydraulic equivalent of Ohm's law, portal pressure is determined by blood flow and resistance. Therefore, the pathophysiology of PHTN can be attributed to increased blood flow, increased vascular resistance, or a combination of both (2). Liver sinusoidal endothelial cells (LSECs), which form the permeabilized barrier of liver sinusoids, are critical regulators of hepatic microcirculation and portal pressure (3). LSECs have been shown to initiate sinusoidal remodeling during the progression of PHTN (1). When exposed to liver injury, liver sinusoids are remodeled, with the loss of LSEC fenestrae and formation of an organized basement membrane (a process termed capillarization) (4), as well as sinusoidal angiogenesis (5). Capillarized sinusoids with basement membrane formation contribute to sinusoidal stiffness, which leads to increased hepatic vascular resistance and the development of PHTN (1). Meanwhile, the capillarized LSECs have the phenotype of common endothelial cells, which can form new blood vessels from preexisting vascular beds, a process termed angiogenesis (6, 7). Increased blood flow caused by angiogenesis in the intrahepatic circulation contributes to PHTN. However, the mechanisms underlying sinusoidal remodeling are not well understood.

Inflammatory signaling also contributes to PHTN through effects on sinusoidal remodeling (5). Prior publications from our group and others showed that inflammatory stimulation (8, 9), including that by tumor necrosis factor-α (TNFα), leads to the loss of the LSEC phenotype (9) and to subsequent aberrant angiocrine signaling, which recruits immune cells to liver sinusoids (10-14). Inflammatory stimulation by lipopolysaccharides promotes the activation and invasion of LSECs, which contributes to angiogenesis and PHTN (15).

Dysfunctional LSECs after inflammatory insult remodel liver sinusoids by promoting hepatic vascular resistance and angiogenesis during the development of PHTN (8, 16). However, the mechanisms by which inflammatory signaling leads to downstream transcriptional regulation in sinusoidal remodeling remain unknown.

Epigenetic mechanisms, such as posttranslational modifications of histone, are involved in transcriptional regulation in human health and disease. Histone marks indicate the activity of the target gene or regulatory elements (17). For example, the research on liver fibrosis shows that trimethylation of histone H3 at lysine 4 (H3K4me3) is common at the promoter region of an active gene, and single methylation of histone H3 at lysine 4 (H3K4me1) is seen at enhancer regions, whereas histone H3 acetylation at lysine 27 (H3K27ac) is noted at both enhancer and promoter regions of active genes (18). Epigenome editing is a way to manipulate gene expression without editing the DNA sequences. The epigenome editing approach CRISPRi-dCas9-KRAB (clustered regularly interspaced short palindromic repeat interference, based on the fusion of nuclease-deactivated Cas9 [dCas9] to the Krüppel-associated box [KRAB]) has become a widespread method to manipulate targeted gene expression because of its high efficiency, specificity, and ease of use (19-21). dCas9 fusion with the epigenetic repressor domain KRAB (dCas9-KRAB) recruits histone methyltransferases (eg, for H3K9me3) to the enhancer or promoter region of the targeted gene under the guidance of single-guide RNA (sgRNA) to promote a regressive effect (22). Prior work from our group has shown the efficiency and mechanism of dCas9-KRAB on repressing chemokine expression via recruiting histone marks to the super enhancer and promoter regions of genes *in vitro* (12, 14). Given that dCas9-KRAB manipulates gene expression without editing DNA sequences, recent studies focus on this epigenome editing technology and its potential clinical application. However, the efficiency of the dCas9-KRAB system *in vivo*, as well as determination of targeted gene function *in vivo*, remains unclear.

Basement membrane—network-forming extracellular matrix (ECM) between endothelial cells and the underlying interstitial tissue—provides a scaffold supporting the surrounding cells and tissues (23). Interestingly, healthy liver sinusoids lack basement membrane, which permits sinusoidal cross-talk. However, sinusoidal basement membrane becomes noticeable upon chronic liver injury. The formation of basement membrane underneath LSECs impedes cellular communication and aggravates liver dysfunction. Collagen type IV (COL4), the major component of basement membrane, has an integral role in its formation and vascular homeostasis (24). The cell type responsible for COL4 production in the liver is unclear, as is the regulation and function of COL4 in the context of liver injury.

In this study, we identified a significant relationship between COL4 deposition and the severity of PHTN. Through single-cell RNA sequencing (scRNA-Seq) studies, we show that LSECs produce COL4, which is under the regulation of the TNFα–nuclear factor–κB (NF-κB) signaling axis. Moreover, epigenetic repression of enhancer-promoter interactions silences COL4 gene expression via a CRISPRi-dCas9-KRAB approach. Furthermore, in mice with COL4 gene mutation or CRISPRi-dCas9-KRAB–mediated COL4 gene repression, we show that LSEC-derived COL4 contributes to the development of PHTN. Mechanistic studies indicate that COL4 promotes sinusoidal resistance through LSEC capillarization and basement membrane formation, as well as by supplying a platform for collagen type I (COL1) binding and assembly. Moreover, COL4 contributes to sinusoidal angiogenesis by activating angiogenic sprouting of LSECs. Taken together, our results indicate a critical role for LSEC-derived COL4 in sinusoidal remodeling and PHTN.

Results

COL4 is upregulated in human and mouse fibrotic livers

Liver cirrhosis and its complication PHTN are associated with the formation of ECM, for which collagens are the core components that provide structural support. Several types of collagens are involved in liver fibrosis and PHTN (25). Of these, fibril-forming COL1 is the most abundant during liver fibrosis (26, 27). Network-forming COL4—a heterotrimer containing 2 α1 chains and 1 α2 chain—is the main constituent of basement membrane of the vessels and is noted in fibrotic livers (24).

To examine changes in collagen expression in liver samples of patients with PHTN, we performed RNA-Seq analysis of human alcohol-induced cirrhotic and normal livers. We identified 950 upregulated genes and 761 downregulated genes in human cirrhotic livers compared with normal livers (Supplementary Figure 1). Among the differentially expressed genes, a wide array of collagen genes showed increased expression, of which *COL1A1*, *COL4A1*, and *COL4A2* (the genes for the COL1 α1 and COL4 α1 and α2 chains, respectively) were most notably overexpressed in cirrhotic livers (Figure 1A). To better quantify the amounts of these collagens, we then used Integrative Genomics Viewer software (Broad Institute) to visualize the normalized expression level of these collagens in healthy and cirrhotic livers (Figure 1B). Other than *COL1A1*, *COL4A1* and *COL4A2* had some of the highest reads per kilobase per million mapped reads (RPKM) in cirrhotic livers. These data reveal that *COL4A1* and *COL4A2* are not only the most upregulated collagen genes, but two of the top expressed collagens in cirrhotic liver. To validate our observation, we performed immunofluorescence (IF) co-staining with COL4 and LSEC marker LYVE1. This showed increased COL4 expression in human cirrhotic livers compared with healthy livers (Figure 1C). COL4 positive areas in liver sinusoids were near LYVE1 positive areas in both human healthy and cirrhotic livers. The peak intensities and number of peaks and ratio for COL4 and Lyve1 are approximately equal. Consistent with the results in human livers, we noted a similar increase in COL4 expression in a carbon tetrachloride (CCl_4)-induced mouse model of liver fibrosis (Figure 1D). COL4 was highly overlapped with LYVE1 positive areas in both healthy and fibrotic livers. Taken together, these data indicate that LSEC-derived COL4 is upregulated with the development of liver fibrosis in human and mouse livers.

LSECs are the primary source of COL4 in healthy and fibrotic livers

Given the increased expression of COL4 in fibrotic livers, we sought to determine the predominant cell type producing COL4 in the liver and assess changes in its expression during the development of liver fibrosis. We performed scRNA-Seq analysis using samples from normal and CCl_4-induced fibrotic mouse livers. All cell types were identified based on previously published conserved genes (28). Analysis using t-distributed stochastic neighbor embedding showed 17 clusters, which corresponded to hepatocytes, endothelial cells, hepatic stellate cells (HSCs), cholangiocytes, Kupffer cells, and other immune cells. Here, *Lyve1* (Figure 2A) were markers for LSECs, and *Pdgfra* and *Pdgfrb* were markers for HSCs (Supplementary Figure 2A). Therefore, clusters 2 and 11 were identified as LSECs, and cluster 5 was identified as HSCs. We then confirmed that *Col4a1* and *Col4a2* were mainly expressed by LSECs and HSCs. Furthermore, LSEC-derived *Col4a1* and *Col4a2* expression levels were higher after CCl_4 administration per violin plots, which was not the case for HSCs (Figure 2B).

LSECs account for 20% of liver-resident cells (29), more plentiful than the 5% of HSCs among liver-resident cells (30). Therefore, we analyzed the percentage of cells expressing COL4 gene in fibrotic mouse livers, $\log_2$ fold change of gene expression in fibrotic vs healthy mouse livers, and adjusted $P<0.05$.

This method identified *Col1a1* and *Col3a1* as most increased in HSCs (Supplementary Figure 2B-C) and *Col4a1* and *Col4a2* as the most upregulated collagens in LSECs (Figure 2C). In contrast, we observed that sinusoidal COL4, which displayed a continuous staining pattern within the sinusoids, was near αSMA, which exhibited a scattered staining pattern around the sinusoids. However, there was no significant co-localization between the two in normal human or fibrotic liver tissues (Supplementary Figure 2E-F). Similarly, PDGFRβ staining exhibited scattered pattern around the sinusoidal COL4. The peak patterns and numbers for αSMA and PDGFRβ are different compared to sinusoidal COL4. This observation suggests that COL4 production is primarily attributed to LSECs rather than HSCs. In addition, analysis of public datasets revealed that LSECs were the main cellular source of COL4 in the human liver (Supplementary Figure 3A, FANTOM5 database; https://fantom.gsc.riken.jp/zenbu/gLyphs/#config=FANTOM5_promoterome_hg19;loc=hg19::chr10:104151762..104164391+), as well as in the mouse liver (Supplementary Figure 3B-C) (31) and accounted for COL4 upregulation in a murine nonalcoholic steatohepatitis model (Supplementary Figure 3D) (32). These public data are consistent with our scRNA-Seq findings.

We then further confirmed the contribution of LSECs and HSCs on COL4 expression during the progression of liver fibrosis and PHTN utilizing primary LSECs and HSCs isolated from mice injected with olive oil or CCl_4. As compared to olive oil control, the expression of *Col4a1* and *Col4a2* was increased in LSECs from CCl_4 fibrotic livers (Figure 2D). However, the expression of *Col4a1* and *Col4a2* in HSCs did not change, which is consistent with our scRNA-Seq data (Figure 2B). In summary, LSECs are the predominant cell type producing COL4 in healthy and fibrotic livers.

TNFα induces COL4 expression in an NF-κB–dependent manner

Based on the transcriptional differences from scRNA-Seq, we next investigated the transcriptional regulation of *COL4A1* and *COL4A2* in LSECs. RNA-Seq data of human cirrhotic liver from our group identified TNFα as a top upstream regulator by IPA analysis (Supplementary Figure 4). Given that *COL4A1* and *COL4A2* were among the most upregulated collagens in human cirrhotic livers (Figure 1A), we hypothesized that COL4 is regulated by TNFα and has a role in liver fibrosis and PHTN. To test this hypothesis, we treated human LSECs with TNFα and confirmed a substantial increase in mRNA expression of *COL4A1* and *COL4A2* (Figure 3A) in response to TNFα stimulation. NF-κB is an important transcription factor downstream of inflammatory stimuli, including TNFα (33). Analysis of public chromatin immunoprecipitation (ChIP)-Seq data sets showed that NF-κB occupied the bi-directional promoter region and putative enhancer regions of *COL4A1*/*COL4A2* in human umbilical vein endothelial cells after TNFα treatment (Supplementary Figure 5). To assess the potential role of TNFα-NF-κB signaling in COL4 expression, we pretreated human LSECs with celastrol, an NF-κB inhibitor. Celastrol strikingly blocked the effect of TNFα and abrogated the expression of *COL4A1* and *COL4A2* at both the mRNA and protein level (Figure 3B-C). These findings indicate that TNFα upregulates production of COL4 in LSECs in an NF-κB-dependent manner.

Epigenetic repression of the enhancer-promoter interaction silences Col4a1 and Col4a2 gene expression

The enhancer-promoter interaction is the linking of distal enhancers with proximal promoters by chromatin looping; these regions harbor transcription factors, coactivators, RNA polymerase II, and the Mediator complex, to orchestrate gene expression (18, 34). Histone mark signals are reliable indicators of active enhancers and promoters (18, 35). Enhancer activity is critical for cell type-specific and spatiotemporal expression of genes (36). To identify the putative enhancer region of LSEC *Col4a1/Col4a2*, we performed tagmentation-assisted fragmentation of chromatin immunoprecipitation sequencing (TAF-ChIP-Seq) of transcription activation mark H3K27ac on isolated mouse LSECs and then speculated 5 putative enhancer regions in H3K27ac-occupied loci (Supplementary Figure 6A, red rectangles). Interestingly, *Col4a1/Col4a2* gene loci that enriched with H3K27ac and H3K4me1 in mouse livers from public ChIP-Seq datasets, both of which were marks of enhancer regions, highly overlapped with the 5 speculated enhancer regions in our LSEC TAF-ChIP-Seq data (Supplementary Figure 6B). Moreover, this gene loci showed increased H3K27ac occupancy at both the putative enhancer and promoter regions in human cirrhotic liver (Supplementary Figure 7), indicating that transcription of *Col4a1/Col4a2* is activated in cirrhotic liver. Based on the above histone modification marks, these findings identify novel multiple enhancers and promoter of COL4 genes, which might be a target to regulate COL4 gene expression and to investigate the role of COL4 in liver fibrosis and PHTN without editing DNA sequences.

Next, we aimed to explore if disturbing enhancer-promoter interaction could regulate COL4 gene expression and the potential mechanisms. For this, we utilized the CRISPRi-dCas9-KRAB epigenome editing approach. dCas9-KRAB recruits H3K9me3 together with heterochromatin protein 1 to induce heterochromatin, chromatin that is inaccessible to the binding of transcriptional regulators. To find the exact loci in the enhancer and the promoter regions that affect COL4 expression, we used Benchling software (14) to design sgRNAs targeting different loci of *Col4a1/Col4a2*: 10 sgRNAs targeting the bi-directional promoter region and 16 sgRNAs targeting the putative enhancer regions (Supplementary Figure

8A). LSECs were isolated from *dCas9-KRAB/Cdh5*$^{\mathrm{CreERT2}}$ (vascular endothelial cadherin promoter with a CreERT2 coding sequence) mice after *in vivo* tamoxifen administration to induce dCas9-KRAB expression specifically in LSECs (Supplementary Figure 8B). The isolated LSECs were transfected with individual synthetic sgRNAs targeting COL4 promoter. *Col4a1* and *Col4a2* expression was significantly decreased with sg4 and sg5 compared with non-targeting sgRNA (Figure 4A). As a control, the expression of the endothelial cell marker *Pecam1* was unchanged (Supplementary Figure 8C). In addition, sgRNA ER1_1 targeting the putative enhancer region showed the greatest repression of *Col4a1/Col4a2*, whereas the expression of *Pecam1* was unchanged (Figure 4B and Supplementary Figure 8D).

To verify the enrichment of histone marks at the enhancer and promoter regions induced by dCas9-KRAB, we performed ChIP-qPCR to evaluate. The targeting of the promoter region by sgRNAs decreased H3K4me3 enrichment at the promoter region and decreased H3K27ac enrichment at the enhancer region, which suggests that disturbing the promoter interferes with enhancer activity (Figure 4C). Likewise, the targeting of the putative enhancer region by sgRNAs decreased H3K27ac enrichment at the enhancer region and H3K4me3 enrichment at the promoter region (Figure 4D). This indicates that these regions are likely the enhancers for *Col4a1/Col4a2* transcription, and that the enhancer interacts with the promoter for gene transcription (Figure 4D). To confirm that this effect of dCas9-KRAB is site-specific, we performed ChIP-qPCR and found that H3K9me3 occupied corresponding sites when sgRNA targeted the promoter or enhancer region (Figure 4E). These results demonstrate that epigenetic repression of the enhancer-promoter interaction by the epigenome editing approach silences COL4 gene expression with high efficacy and specificity *in vitro*, which paves the road for epigenome editing of transcriptional regulatory elements of COL4 genes *in vivo* and the therapeutic potential of COL4 repression in liver fibrosis and PHTN.

LSEC-specific COL4 contributes to PHTN

Given the upregulation of LSEC-derived COL4 in liver fibrosis and PHTN, we aimed to investigate the biological function of COL4 in the liver, which is poorly understood. First, we used a conditional LSEC-specific *Col4a1* mutant mouse in a Cre-dependent manner (37). *Col4a1* mutation was induced by deleting exon 41 (with a floxed DNA sequence under Cre recombinase control) (37) to produce a truncated, dysfunctional COL4 protein (Figure 5A). We detected COL4 expression in liver sinusoids with electronic microscopy via immunogold staining (Figure 5B). In control mice, COL4 was secreted and deposited in the perisinusoidal spaces, whereas *Col4a1* mutation blocked COL4 deposition in liver sinusoids (Figure 5B). This suggests that secreted COL4 is deposited in liver sinusoids and that *Cdh5*$^{\text{CreERT2}}$-induced LSEC mutation of *Col4a1* is effective and subsequently decreases sinusoidal COL4 deposition.

Next, we investigated the role of LSEC-derived COL4 in PHTN using LSEC-specific *Col4a1* mutant mice. After 6-week CCl_4 administration to induce PHTN, portal pressure was increased 2-fold in the littermate control (*Col4a1*$^{\text{fl/wt}}$) mice. In contrast, portal pressure decreased significantly (36%) in the *Col4a1*$^{\text{fl/wt}}$/*Cdh5*$^{\text{CreERT2}}$ mice compared with *Col4a1*$^{\text{fl/wt}}$ mice (Figure 5C). During the development of PHTN, intensified hepatic vascular resistance blocks splanchnic blood flow to liver, which leads to congestion of splanchnic circulation (35). Therefore, we measured spleen weight in control and mutant mice. Indeed, the ratio of spleen weight to body weight was higher in mice that exhibited PHTN by CCl_4 administration. In contrast, the ratio was decreased by 21% in CCl_4-treated *Col4a1*-mutated mice, which was consistent with the change in portal pressure

(Figure 5D). Taken together, our data suggest that LSEC-specific COL4 has an important role in PHTN.

Vascular permeability influences blood pressure regulation; decreased vascular permeability increases vascular resistance and thus increases blood pressure (38). To examine whether COL4-induced basement membrane affects sinusoidal permeability, we performed *in vivo* permeability assays by injecting 4-kDa fluorescein isothiocyanate (FITC)-dextran via the tail vein in mice administered olive oil (control) or CCl_4. Sinusoidal permeability was assessed by determining FITC-dextran endocytosed by hepatocytes. The assays showed FITC-dextran at the sinusoidal barrier in the CCl_4-injected *Col4a1*$^{fl/wt}$ (control) mice (Figure 5E). The amount of FITC-dextran endocytosed by hepatocytes was significantly decreased in CCl_4-injected *Col4a1*$^{fl/wt}$ mouse liver but was recovered in CCl_4-injected *Col4a1*$^{fl/wt}$/*Cdh5*^{CreERT2} liver. The data suggest that COL4 restricts sinusoidal permeability due to LSEC capillarization and formation of basement membrane. Thus, LSEC-derived COL4 appears to impair sinusoidal permeability and thus propagates PHTN.

LSEC-derived COL4 promotes sinusoidal resistance during the progression of portal hypertension

Previous studies have shown CD34 to be a potent marker of LSEC capillarization (39, 40). Given that LSECs are the cellular source of COL4, which has a critical role in PHTN, we hypothesized that COL4 promotes sinusoidal remodeling via induction of sinusoidal resistance. To test that, we first detected capillarization (*Cd34*) and LSEC (*Lyve1*, *Stab1*) markers from isolated mouse LSECs by qPCR. These assays confirmed that CCl_4-induced LSECs showed a capillarized phenotype with increased *Cd34* and decreased *Lyve1* and *Stab1* mRNA levels. In contrast, *Col4a1*-mutated LSECs with CCl_4 administration maintained the LSEC phenotype (Figure 6A). Likewise, CD34 expression was increased and LYVE1 expression was strikingly decreased in human cirrhotic liver as shown by IF staining, which indicates loss of the LSEC phenotype with the development of PHTN (Supplementary Figure 9).

We then directly investigated the ultrastructure of liver sinusoids with electron microscopy. Although the LSECs from healthy livers showed characteristic fenestrae (Figure 6B, red arrow) and the presence of a sieve plate (Figure 6C, red star), LSECs from cirrhotic livers were defenestrated and the sieve plate was absent (Figure 6B and C), underneath which obvious basement membrane was observed (Figure 6B, black arrow). Although the perisinusoidal spaces were narrow and without obvious basement membrane deposition, they were widened as a result of deposition of basement membrane (Figure 6B, black arrow) and other collagens (Figure 6B, black star). In contrast, *Col4a1*-mutant mice with CCl_4 injection showed an absence of COL4 expression and basement membrane formation in liver sinusoids (Figure 6B and C). This evidence suggests that COL4 is an important mediator for LSEC capillarization. The remodeled sinusoids contribute to sinusoidal resistance and the development of PHTN.

COL4 supplies a scaffold for COL1 deposition and assembly in liver sinusoids to promote sinusoidal resistance

Evidence has shown that COL4, a network-forming ECM, helps form the basement membrane, whereas COL1, a fibril-forming ECM, is secreted by activated HSCs and deposited in the perisinusoidal spaces. By IHC staining of COL1 (Figure 7A), COL1 deposition was evident in CCl_4-injected mouse liver sinusoids, but the absence of basement membrane formation due to *Col4a1* mutation accompanied decreased COL1 deposition in liver sinusoids. Therefore, we hypothesized that basement membrane supplies a scaffold for COL1 deposition and assembly in the perisinusoidal spaces. To test that, we performed IF staining followed by 3D super-resolution Airyscan (Zeiss) microscopy and reconstructed the images via Imaris Microscopy Image Analysis Software (Oxford Instruments) to illustrate the colocalization of COL4 and COL1 in liver sinusoids. Both COL4 and COL1 were enhanced in liver sinusoids but were distributed differently. A portion of COL1 was structurally surrounded and supported by COL4 via reconstructed images (Figure 7B and Supplementary Video 1). In contrast, sinusoidal COL1 showed a patchy and discontinuous pattern without the structural support of network-forming COL4 in LSEC-specific *Col4a1*-mutated liver sinusoids (Figure 7B and Supplementary Video 1). These findings indicate that COL4 may supply a scaffold for COL1 deposition, which contributes to firm ECM and sinusoidal resistance.

COL4 contributes to sinusoidal remodeling by activating angiogenic sprouting of LSECs

Pathologic angiogenesis in fibrotic liver increases intrahepatic blood flow, thus aggravating PHTN (6, 41). To examine the effect of COL4 on angiogenesis, we isolated mouse LSECs from *Col4a1*$^{fl/wt}$ and *Col4a1*$^{fl/wt}$/*Cdh5*^{CreERT2} mice and confirmed that CCl_4-injected LSECs transformed into an angiogenic sprouting phenotype, as indicated by filopodial tip cells with abundant COL4 synthesis in the endoplasmic reticulum (ER) and secretion via intracellular vesicles (Figure 8A). In contrast, the *Col4a1* mutation in LSECs inhibited secretion of COL4 and maintained the LSEC phenotype, blocking the activation of LSECs (Figure 8A). These findings suggest that COL4 activates LSEC angiogenic sprouting.

In addition, *Col4a1* mutation led to dysfunctional COL4 being retained in the ER (Figure 8A), which has also been shown previously (37). To further confirm that maintenance of the LSEC phenotype is not the result of dysfunctional

COL4 retention in the ER, we used an *in vitro* model to knock down *COL4A1* gene expression in primary human LSECs by small interfering RNA (siRNA) to verify the role of COL4 in angiogenesis. *COL4A1* siRNA showed high efficiency, as reflected by depletion of *COL4A1* mRNA (Figure 8B). We then noted that COL4 was secreted extracellularly and organized into COL4 bundles and tubules in human LSECs transfected with *scramble* siRNA after TNFα treatment. However, COL4 bundles and tubules were inhibited by *COL4A1* gene knockdown, as shown by decreased branch points (Figure 8C), which suggests that COL4 is essential for LSEC-driven angiogenesis. These results demonstrate that COL4 stimulates LSEC angiogenic sprouting, which increases blood flow in the liver and subsequently propagates the development of PHTN.

Epigenetic repression of LSEC-derived COL4 alleviates PHTN

To confirm the role of the interaction between specific COL4 enhancer and promoter loci identified in Figure 4 on portal hypertension, we utilized the CRISPRi-dCas9-KRAB epigenome editing *in vivo*. We used adeno-associated virus (AAV) encoding the sgRNAs sg4 and sg5, which showed high efficacy in targeting the bi-directional promoter, disturbing enhancer activity and silencing *Col4a1* and *Col4a2* expression in cultured primary mouse LSECs (Figure 4A). *dCas9-KRAB/Cdh5*^{CreERT2} mice were first injected with tamoxifen to induce LSEC-specific dCas9-KRAB expression before AAV delivery. We then administered the sgRNA AAVs systemically to 8-week-old *dCas9-KRAB/Cdh5*^{CreERT2} mice via tail vein injection. LSECs were isolated 2 weeks after AAV-sg delivery and the repression of *Col4a1* and *Col4a2* mRNA expression was confirmed (Supplementary Figure 10).

We next injected the mice with olive oil, or CCl_4 for establishment of the PHTN model (Figure 9A). CCl_4 treatment increased portal pressure by 70% in mice administered with the AAV vector containing a non-targeting control sgRNA, which was abrogated when mice were administered with AAV-sg4 and AAV-sg5 (Figure 9B).

To confirm the role of COL4 in sinusoidal remodeling, we first performed staining showing that sinusoidal COL4 deposition was blocked in mice with administration of AAV-sg4 and AAV-sg5 in addition to CCl_4 (Figure 9C and Supplementary Figure 11). Consistent with the data, robust Cd34 expression was noted in liver sinusoids in mice with PHTN, which was absent in mice with AAV-sg4 and AAV-sg5 administration (Figure 9D and Supplementary Figure 12). We further confirmed abrogation of *Col4a1* and *Col4a2* and *Cd34* gene expression in isolated LSECs from mice administered with AAV-sg4 and AAV-sg5 (Figure 9E and F). These results demonstrate high efficiency of AAV delivery and the repressive effect of dCas9-KRAB on the COL4 genes in LSECs *in vivo*. More importantly, this evidence confirms the pivotal role of COL4 in sinusoidal remodeling and PHTN *in vivo*.

Discussion

PHTN is a severe complication of chronic liver disease and a pivotal determinant of disease prognosis and outcomes. Although substantial progress has been made in treating the various causes of chronic liver disease, few therapies are available for the management of PHTN (2, 42). In this study, we provide insights regarding the role of COL4 in the pathogenesis of PHTN. Several observations stand out from our study: 1) COL4 expression is markedly increased in both human and mouse fibrotic livers; 2) LSECs are the cellular source of COL4 in healthy and fibrotic livers, and LSEC-derived COL4 is under the transcriptional regulation of the TNFα-NF-κB signaling axis; 3) epigenetic repression of the enhancer-promoter interaction silences COL4 gene expression; 4) COL4 induces sinusoidal resistance and angiogenesis, the remodeled sinusoid propagating PHTN; and 5) epigenetic repression of COL4 using CRISPRi-dCas9-KRAB epigenome editing *in vivo* attenuates PHTN. Taken together, our findings elucidate the mechanism of LSEC-derived COL4 upregulation and the role of COL4 in sinusoidal remodeling and PHTN.

COL4, a major component of basement membrane, has been studied extensively. It has a critical role in different disease states including intracerebral hemorrhages (37) and glomerular diseases (24, 43), but its role in liver diseases remains elusive. Although a few studies have shown increased COL4 expression in cirrhotic liver (5, 44), the function and cellular source of COL4 in the liver are incompletely explored. Here, we showed that the expression of COL4 increases with the progression of liver cirrhosis and PHTN in human and mouse liver by using an unbiased transcriptome approach and in combination with hypothesis-driven studies. Few studies have shown the source of COL4 in the liver (44). By analyzing our scRNA-Seq data and publicly available data sets, we demonstrated that LSECs are the primary source of COL4 and further confirmed its increase in LSECs from mice with PHTN. Although we showed that HSCs also produce COL4, the expression level is much lower and unchanged between healthy and diseased liver. In contrast, HSCs are the main source of COL1 in cirrhotic liver from our scRNA-Seq data and previous publications (25, 26, 39). Additionally, we conducted a detailed assessment of our scRNA-seq data of olive oil and CCl_4 mouse livers. Our findings indicated that MMP14, secreted by LSECs, as well as MMP8 and MMP23 from immune cells, displayed no significant alterations in their expression levels. These combined results suggest that the increased deposition of COL4 in both human and mouse fibrotic livers may be the consequence of elevated COL4 expression rather than degradation. In summary, our study is novel to identify LSECs as the cellular source of COL4 in the liver.

Given the marked increase in COL4 expression in cirrhotic liver and its important role in PHTN, we aimed to identify the signaling pathways leading to this upregulation. TNFα is the top upstream regulator in the pathogenesis of liver cirrhosis (11) and contributes to loss of the LSEC phenotype (15). However, the underlying mechanism remains elusive. The current study used an LSEC-specific *Col4a1*-mutated and *Col4a1/Col4a2*-repressed model to show that TNFα-NF-κB signaling leads to LSEC capillarization in a COL4-dependent manner. Nevertheless, the interaction of NF-κB with epigenetic factors to modulate the expression of *Col4a1* and *Col4a2* in LSECs is mechanistically unexplored.

Histone modifications have key roles in enhancer-promoter interactions and are reliable indicators of transcriptional regulatory elements (45). CRISPRi-dCas9-KRAB is a useful approach to epigenetically regulate targeted gene expression with the help of sgRNA (22). We identified decreased enhancer activity when sgRNA targeted the COL4 promoter, as well as decreased promoter activity when sgRNA targeted the COL4 enhancer, shown by the absent enrichment of H3K27ac and H3K4me3 at the corresponding site. Our study indicates that epigenetic repression of the enhancer-promoter interaction silences COL4 gene expression. Given the efficacy and mechanisms of CRISPRi-dCas9-KRAB on COL4 repression, we then used a *dCas9-KRAB/Cdh5*$^{\mathrm{CreERT2}}$ mouse model together with AAV-sgRNA targeting the *Col4a1/Col4a2* bi-directional promoter to elucidate the function of COL4 in sinusoidal remodeling and PHTN. The data demonstrated that efficient repression of COL4 indeed maintained sinusoidal structure and portal pressure. It's important to note that while CRISPR-Cas9 holds tremendous therapeutic potential, it is still a rapidly evolving field, and ongoing research aims to address safety concerns and improve the precision of the technology.

LSECs maintain sinusoidal communications and homeostasis via angiocrine signaling (46). However, during chronic liver injury LSECs dedifferentiate to a capillarized phenotype and secrete fibrogenic factors, such as transforming growth factor β and platelet-derived growth factor, which leads to quiescent HSC contraction and activation and subsequently initiates liver cirrhosis and PHTN (5, 47-49). In addition, LSECs induce liver cirrhosis and PHTN by recruiting infiltrated neutrophils in a CXCL1-dependent manner (13) and infiltrated proinflammatory macrophages in a CCL2-dependent manner (12). These inflammatory macrophages produce TGFβ to activate HSCs, as well as TNFα to defenestrate LSEC, which contributes to liver fibrosis and portal hypertension. All these studies demonstrate the pivotal role of LSECs in the progression of liver fibrosis and PHTN by mediating sinusoidal cross-talk. Whereas sinusoidal crosstalk driven by canonical nitric oxide signaling in portal pressure is well established (47), other mechanisms of LSECs regulating portal pressure are poorly understood. In the current study, we demonstrated that a decrease in functional COL4 production in LSECs lowers the portal pressure in our mouse models of COL4 gene mutation and repression. This suggests a role of LSEC-derived COL4 in PHTN.

The pathobiology of PHTN involves changes in hepatic architecture caused by increased intrahepatic vascular resistance and increased blood flow (42). HSC activation and subsequent ECM deposition distort the liver vascular anatomy and increase liver stiffness, which leads to increased hepatic vascular resistance (25, 50). In this study, we showed that organized, continuous basement membrane formation due to capillarized LSECs increases sinusoidal resistance. Moreover, COL4-enriched basement membrane acts as a scaffold for COL1 deposition in liver sinusoids, which increases sinusoidal stiffness. The absence of COL4 leads to lack of a platform for COL1 deposition in liver sinusoids; unstable fibrillar collagens, such as COL1, without assembly and deposition, might in turn be degraded (51). The glycoprotein fibronectin binds and interacts with collagen and is involved in collagen assembly and deposition (52). A previous publication showed spatial accumulation of fibronectin adjacent to the basement membrane (53). Currently, the relationship between COL4 and COL1 is largely unknown, and fibronectin is speculated to be a mediator linking COL1 on a COL4 scaffold, but this needs further investigation. Collectively our data indicate that LSEC-derived COL4 mediates LSEC capillarization and basement membrane formation, contributing to sinusoidal resistance during the development of PHTN.

Besides increased sinusoidal resistance, angiogenesis-induced blood flow in the liver contributes to PHTN. Intrahepatic angiogenesis occurring after liver injury drives pathologic sinusoidal remodeling and increases the vascular volume, further propagating PHTN (16, 54, 55). Studies have demonstrated that inhibition of vascular endothelial growth factor is beneficial for attenuating intrahepatic vascular remodeling and PHTN (56). Our study indicates that COL4 is an important factor mediating angiogenesis, as shown by angiogenic sprouting of mouse and primary human LSECs. COL4 has been shown to be involved in pathological retina angiogenic sprouting (57) and lung endothelial cell angiogenesis in vivo (58). In that work, the authors observed the number of filopodia at the angiogenic front were decreased along with the reduction of functional secreted COL4 (57), and further confirmed that COL4 contributes to tube formation of lung endothelial cell through integrin-FAK signaling by knockdown expression of COL4 (58). Taken together, our data show that COL4 directly affects portal pressure by sinusoidal resistance and angiogenesis. In conclusion, our work implicates the mechanisms of LSEC-derived COL4 regulation and its role in the pathophysiology of PHTN. COL4 can potentially become a therapeutic target in PHTN.

Materials and Methods

Sex as a biological variable

In this study, we included both female and male individual. The results showed consistency across genders, and no distinctions were made based on sex in the analysis or interpretation of the findings.

In vivo experiments

Col4a1$^{fl/wt}$ mice were kindly provided by Dr. Douglas B. Gould at the University of California, San Francisco. *Col4a1*$^{fl/wt}$ mice were crossed with *Cdh5*^{CreERT2} mice to generate *Col4a1*$^{fl/wt}$/*Cdh5*^{CreERT2} mice. Mice at 6 to 7 weeks old were intraperitoneally injected with tamoxifen (75 mg/kg per day) for 5 consecutive days to induce LSEC-specific *Col4a1* mutation. To induce liver fibrosis–related PHTN, CCl_4 (Sigma-Aldrich #319961) at 1 μL/g of body weight was intraperitoneally administered twice per week for 6 weeks. Mice were humanely killed 48 hours after the last injection.

dCas9-KRAB mice were purchased from The Jackson Laboratory (#033066). *dCas9-KRAB* mice were crossed with *Cdh5*^{CreERT2} mice to obtain *dCas9-KRAB/Cdh5*^{CreERT2} mice. Tamoxifen was administered to induce dCas9-KRAB expression in LSECs. sgRNA targeting the bi-directional promoter or enhancer region for the *Col4a1* and *Col4a2* genes was delivered into *dCas9-KRAB/Cdh5*^{CreERT2} mice via the tail vein before the 6-week CCl_4 injections.

Portal pressure measurement

The mouse portal vein was cannulated with a 24-gauge catheter attached to a pressure transducer and connected to a Digi-Med Blood Pressure Analyzer (BPA-400) to measure portal pressure.

Liver sinusoid permeability assay

Mice were anesthetized with isoflurane. Permeability of the liver sinusoids was measured by FITC-dextran injection. Briefly, 200 μL of a 0.01 mg/mL 4-kDa FITC-dextran solution in saline was injected via the tail vein. Five minutes later, mice were killed, and the liver was harvested, embedded in optimal cutting temperature compound (Tissue-Tek O.C.T. Compound; Sakura #4583), and flash-frozen on dry ice. The frozen liver was cut into 7-μm thick sections on a cryostat (Leica Microsystems) and mounted on glass slides. Liver sinusoid permeability was analyzed by determining the amount of FITC-dextran endocytosed by hepatocytes with Image J software.

Mouse LSEC isolation and culture

Mouse LSECs were isolated from *Col4a1*$^{\mathrm{fl/wt}}$, *Col4a1*$^{\mathrm{fl/wt}}$/*Cdh5*$^{\mathrm{CreERT2}}$, and *dCas9-KRAB/Cdh5*$^{\mathrm{CreERT2}}$ mice as previously described (59). Briefly, mice were anesthetized with isoflurane before the liver was perfused with phosphate-buffered saline (PBS) containing proteases (Roche #25551121) and collagenase P (Roche #11249002001). The perfused liver was homogenized and filtered through a 70-μm cell strainer to obtain a single-cell suspension. Anti-CD146 microbeads (Miltenyi Biotechnology #130-092-007) then were used to purify LSECs according to the manufacturer's protocols. The purified LSECs were plated on a COL1-coated dish and glass chamber and cultured in Endothelial Cell Medium (ScienCell Research Laboratories #1001) for 4 hours. The cells were harvested for further analysis.

Cell treatment and siRNA transfection

Human LSECs (ScienCell Research Laboratories #5000) were cultured according to manufacturer instructions. To study COL4 expression, low-passage cells were starved with low-serum medium (0.5% fetal bovine serum [FBS] in basal endothelial medium) for 2 hours followed by treatment with NF-κB inhibitor (celastrol, 2μM; Sigma #C0869) for 2 hours. Next, human recombinant TNFα (20 ng/mL; PeproTech, #300-01A) was added to low-serum medium and incubated with cells for 4 to 24 h before cells were collected for further analysis (qPCR and IF staining). For siRNA transfection, human LSECs at 70% confluence were transfected with *COL4A1* or *scramble* siRNAs (ON-TARGETplus SMARTpool; Dharmacon, Horizon Discovery) using the Lipofectamine RNAiMAX Transfection Reagent (ThermoFisher) according to manufacturer instructions. Cells were collected after 48 h of transfection.

TAF-ChIP-Seq analysis

TAF-ChIP-Seq was performed at the Epigenomics Development Lab at Mayo Clinic by using antibodies against histone mark H3K27ac. Briefly, mouse LSECs were isolated and cross-linked with 1% formaldehyde for 10 min, followed by quenching with 125mM glycine for 5 min at room temperature and by washing with PBS. The pellets were resuspended in lysis buffer and incubated on ice before sending them to the epigenomics lab.

RNA-Seq and analysis

RNA-Seq was performed on whole liver from human samples of healthy and alcohol-induced cirrhotic liver at the Mayo Clinic Center for Individualized Medicine Medical Genome Facility. Some of the raw RNA-Seq data have been previously published by our group and are available on the GEO database (GSE155907). The detailed protocols were described in a previous paper (14).

Single-cell RNA-Seq and analysis

The single-cell RNA sequencing analysis depicted in Figure 2B was based on a pooling strategy that combined purified hepatocytes (~1/3 of the entire cell population), enriched HSCs (~1/3), and other non-parenchymal cells (NPCs) (~1/3), which encompassed cell types like LSECs, Kupffer cells, and others. It is important to note that this pooling strategy does not reflect the actual cell number ratios, particularly concerning LSECs and HSCs, *in vivo* and rather results in an over-representation of HSCs. HSCs isolation has been described previously (27). Mouse hepatocytes and liver nonparenchymal cells were isolated after the mice underwent 6 weeks of administration of olive oil or CCl_4. Briefly, livers were perfused with PBS containing proteases and collagenase P before they were homogenized and filtered through a 70-μm cell strainer to obtain a single-cell suspension. The cell suspension was centrifuged at 50×g for 3 min to remove hepatocytes and save for sequencing. The supernatants were pelleted at 500×g for 5 min and resuspended in Endothelial Cell Medium. Samples were then prepared according to the Chromium Single Cell 3′ v2 Reagent Kit (10X Genomics) user guide. Briefly, liver nonparenchymal cells were pelleted and resuspended in PBS + 0.04% bovine serum albumin to 1,000 cells/μL. Cell viability was evaluated with trypan blue, and cell number was confirmed with an automated cell counter. Samples were loaded onto the Chromium Single Cell-A chip (10X Genomics) to convert polyadenylated mRNA into cDNA. cDNA was amplified by PCR for library generation. Samples were sequenced on a HiSeq 2500 system (Illumina) at the Mayo Clinic Center for Individualized Medicine Medical Genome Facility with the following run parameters: read 1, 26 cycles; read 2, 98 cycles; index 1, 8 cycles. scRNA-seq datasets are annotated by CellMarker 2.0 databases (https://doi.org/10.1093/nar/gkac947).

Real-time PCR

RNA extraction from cells and liver tissues was performed with the RNeasy Mini Kit (Qiagen #74104) according to the manufacturer's protocols. RNA 500 ng was used for cDNA synthesis with oligo primer and dNTPs using SuperScript III First-Strand Synthesis System (Invitrogen #18080-051) after RNA quantification by spectrophotometry (NanoDrop; ThermoFisher). qPCR was performed using iTaq Universal SYBR Green Supermix (Bio-Rad #1725120) according to the manufacturer's instructions. For murine samples, mRNA levels were normalized to the housekeeping gene β-actin. For human samples, mRNA levels were normalized to the housekeeping gene GAPDH. Primer sequences are listed in Supplementary Table 1.

Western blot assay

Cells or liver tissues were lysed in RIPA buffer (Cell Signaling Technology, Inc 9806S) with Complete, Mini, EDTA-free protease inhibitor cocktail (Roche #4693159001). Equal amounts of protein for cell lysates (15 μg) or liver lysates (30 μg) were loaded onto SDS-PAGE gel and transferred to nitrocellulose membrane. The membrane was incubated overnight with primary antibodies after blocking with 5% blotting-grade blocker (Bio-Rad #1706404) for 1 h. Primary antibodies were used to detect HSC70 (Santa Cruz Biotechnology, Inc #sc-7298) and CAS9 (EnCor Biotechnology Inc; #MCA-3F9). The signal of blot was developed and detected using chemiluminescence substrate (Western Blotting Luminol Reagent; Santa Cruz #sc-2048 or Immobilon Crescendo Western HRP substrate; Millipore #WBLUR0100). HSC70 was used as the loading control, and the results were quantified with Image J software.

IHC staining

Mouse livers were fixed in 10% formalin, embedded in paraffin, and cut into 5-μm sections. Slides were deparaffinized, and antigen retrieval was performed (IHC-Tek; IHC WORLD #IW-1000) before blocking in 10% FBS for 1 h at room temperature and incubating overnight at 4 °C with primary antibodies: anti-COL1 (Southern Biotech #1310-01) or anti-CD34 (Abcam ab81289). After incubation with biotinylated secondary antibody (Vector Laboratories #BA-1100) for 1 h at room temperature, slides were treated with VECTASTAIN Elite ABC-HRP Reagent, Peroxidase (Vector Laboratories #PK-7100) for 30 min before treating with DAB Substrate Kit, Peroxidase (Vector Laboratories #SK-4100) for 3 min. Slides were counterstained with hematoxylin and dehydrated in ethanol and xylene. Images were acquired on a histologic microscope at ×20 and ×40 magnification, 6 images per slide.

IF staining

Frozen liver tissues were cut into 7-μm sections and fixed in acetone for 10 min and permeabilized with 0.5% Triton X-100. Slides were blocked in 10% FBS for 1 h at room temperature before being incubated with primary antibody overnight at 4 °C. Primary antibodies and stains used included anti-COL4 (Southern Biotech #1340-01; Abcam #ab19808), anti-COL1 (Southern Biotech #1310-01), anti-CD34 (Abcam ab81289), anti-LYVE1 (R&D Systems #AF2125), Phalloidin-TRITC (Sigma #P1951), anti-COL4a1 (Chondrex, Inc #7070), anti-COL4 (Abcam ab236640), anti-PDGFRβ (Cell Signaling 3169), anti-αSMA (Abcam ab7817), and anti-Hsp47 (Novus Biologicals #NBP1-97491). After incubation with fluorochrome-coupled secondary antibody (Invitrogen, #A11055, #A11057, #A21206, #A11077, #A21202, #A10042) and DAPI, images were visualized on a Zeiss LSM 780 confocal microscope. 3D super-resolution images were visualized on a Zeiss LSM 980 Airyscan microscope and reconstructed and viewed with Imaris image analysis software. Colocalization analysis was done as described previously (60). Three sinusoidal areas were selected for analysis. Fluorescent intensity peaks and ratio of green fluorescence vs red fluorescence were quantified by Zen image browser at four straight arrows as shown in the schema of hepatic sinusoid (Supplementary Figure 2D).

sgRNA design and transfection

sgRNA sequences targeting the bi-directional promoter or putative enhancer region of *Col4a1/Col4a2* were designed using public Benchling software and synthesized by Horizon Discovery. For isolated LSECs from *dCas9-KRAB/Cdh5*^{CreERT2} mice, synthetic sgRNA was transfected using DharmaFECT Duo Transfection Reagent (Horizon Discovery) according to the manufacturer's protocols for 18 h before mouse recombinant TNFα was administered for 24 h. The cells then were harvested for qPCR or ChIP-qPCR analysis. The sgRNA sequences are listed in Supplementary Table 2.

AAV cloning, production, and delivery

sgRNA 4 (sg4) and sgRNA 5 (sg5), which revealed high efficiency in silencing COL4 gene expression, were selected to clone into the AAV backbone. An AAV backbone encoding sgRNA (pAAV-U6-sgRNA-CMV-GFP) was obtained from Vector Biolabs. An AAV encoding LacZ (pAAV-U6-LacZ-CMV-GFP) was used as the non-targeting control (AAV-non). High-titer AAVs for systemic delivery were produced in serotype AAV2 by Vector Biolabs. *dCas9-*

KRAB/Cdh5^{CreERT2} mice were injected with AAV-sg4 (1×10^{11} viral genomes/mouse), AAV-sg5 (1×10^{11} viral genomes/mouse), or AAV-non (1×10^{11} viral genomes/mouse) via the tail vein using a 31-gauge needle. LSECs were isolated to detect Col4a1 and Col4a2 expression 2 weeks after AAV delivery.

Electron microscopy

Anesthetized mice were perfused with Trump's fixative (Electron Microscopy Sciences #11750) via the portal vein. Dissected liver lobes were subsequently immersed in freshly prepared aldehyde fixative overnight before sending these samples to the Microscopy and Cell Analysis Core at Mayo Clinic for further processing.

Transmission electron microscopy

Tissue was placed into fixative (4% paraformaldehyde + 1% glutaraldehyde in 0.1M PBS, pH 7.2). After fixation, tissue was washed with PBS, stained with 1% osmium tetroxide, washed in distilled water, stained with 2% uranyl acetate, washed in distilled water, dehydrated through a graded series of ethanol and acetone, and embedded in EMbed 812 resin (Electron Microscopy Sciences #14120). After 24 h of polymerization at 60 °C, 0.1-μM ultrathin sections were prepared and poststained with lead citrate. Micrographs were acquired at 80 kV using a JEM-1400 Plus transmission electron microscope (JEOL, Inc) equipped with a Gatan Orius camera (Gatan, Inc).

Scanning electron microscopy

After fixing in Trump's fixative at 4 °C overnight, livers were washed in PBS, rinsed in water, and dehydrated through a graded series of ethanol. It was then critical point dried using carbon dioxide, mounted on an aluminum stub, and sputter-coated with gold-palladium for 90 seconds. Finally, livers were imaged in a

Hitachi S-4700 cold field emission scanning electron microscope at 5-kV accelerating voltage.

Immunogold staining

Livers were first perfused with 0.1% glutaraldehyde and 4% paraformaldehyde in 0.1M PBS for 2 h. The sample was then cryoprotected by immersion in 2.3M sucrose in 0.1M PBS overnight and frozen in liquid nitrogen. Cryosections 5- to 6-µm thick were cut with a Leica cryomicrotome (Leica Microsystems). Samples were incubated overnight at 4 °C with anti-COL4 antibody (Abcam, #ab19808) diluted 1:20 in 10% fetal calf serum/PBS. Sections were then incubated with goat anti-rabbit Ultra Small ImmunoGold secondary antibody (Electron Microscopy Sciences) for 2 h at room temperature. Sections were further fixed in 1% glutaraldehyde for 15 min; then silver enhancement was performed with R-Gent Silver Enhancement Reagents, SE-EM (Electron Microscopy Sciences) for 30 min and postfixed with 1% osmium tetroxide for 30 min. After washing with distilled water, the sections were dehydrated with serial alcohol, infiltrated, and embedded with Spurr resin. The specimens were cut at 90-nm thickness and stained with lead acetate, then viewed at 80 kV using a JEM-1400 Plus electron microscope (JEOL, Inc).

ChIP-PCR

Mouse LSECs were isolated according to the previous protocol. LSECs were transfected with sgRNA and underwent ChIP with the Magna ChIP HiSens Chromatin IP Kit (Millipore MAGNA0025) according to the manufacturer's protocol. Briefly, cells were cross-linked, washed, collected, and lysed with lysis buffer. The nucleus was extracted using nuclear lysis buffer. Chromatin (10 µg per IP reaction) was sonicated, centrifuged, and immunoprecipitated with magnetic beads with antibodies against H3K9me3 (Abcam ab8898), H3K27ac (Abcam ab4729), and H3K4me3 (Diagenode #C15410003). Isotype IgG (Sigma #12-370) was used as control.

Statistical analysis

All data were analyzed with GraphPad Prism software (version 9.0). Data represent mean ± standard error and were analyzed by analysis of variance or a *t* test with post hoc Bonferroni correction. $P<.05$ was considered statistically significant.

Study approval

Human liver samples were collected at Mayo Clinic with institutional approval (IRB 15-008251). All animal experiments were conducted in accordance with guidelines approved by the Mayo Clinic Institutional Animal Care and Use Committee.

Data availability statement:

All relevant data supporting the findings of this study are reported within the article or its supplemental material. The scRNA-Seq data generated in this publication will be available on the GEO database (GSE199064). The TAF-ChIP-Seq data generated in this publication will be available on the GEO database (GSE233284). The RNA-Seq data are available on the GEO database (GSE155907). The ChIP-Seq data are available on the GEO database (GSE155908, GSE31039, GSE53998).

Author contributions: C.G. contributed to study design, animal and cell experiments, data acquisition and analysis, and drafting of the manuscript. U.Y., M. X, A. A, and N.J.S. contributed to genotyping and animal experiments. J.L. and J.S.O. contributed to cell experiments. A.N.C. and E.K. contributed to CRISPR and epigenetic studies. T.S.S. contributed to genomic sequencing studies and associated data analysis. N.W.H. contributed to revision of the manuscript. S.C. contributed to study design, data analysis, intellectual input, and revision of the manuscript. V.H.S. contributed to study design, resources, funding support, revision of the manuscript, and overall study supervision.

Acknowledgment:

This research was supported by funding from the National Institutes of Health (NIH) grants (DK59615, DK136511), National Natural Science Foundation of China (82300711), as well as funding from Mayo Clinic Center for Cell Signaling in Gastroenterology (P30 DK084567). We are grateful to Dr. Douglas B. Gould at the University of California, San Francisco for providing us *Col4a1*$^{fl/wt}$ mice. We are grateful to Huihuang Yan, PhD, at Mayo Clinic for bioinformatics analysis. We are grateful to Trace A. Christensen, MBA; Scott I. Gamb; and Bing Quan Q. Huang, PhD, at Mayo Clinic for electron microscopy support. Alyssa B. Quiggle, PhD, provided editorial suggestions on an earlier draft of the manuscript.

References:

1. Iwakiri Y, Shah V, and Rockey DC. Vascular pathobiology in chronic liver disease and cirrhosis: current status and future directions. *J Hepatol.* 2014;61(4):912-24.
2. Engelmann C, Claria J, Szabo G, Bosch J, and Bernardi M. Pathophysiology of decompensated cirrhosis: portal hypertension, circulatory dysfunction, inflammation, metabolism and mitochondrial dysfunction. *J Hepatol.* 2021;75 Suppl 1:S49-S66.
3. DeLeve LD. Liver sinusoidal endothelial cells and liver regeneration. *J Clin Invest.* 2013;123(5):1861-6.
4. Marrone G, Shah VH, and Gracia-Sancho J. Sinusoidal communication in liver fibrosis and regeneration. *J Hepatol.* 2016;65(3):608-17.
5. Winkler M, Staniczek T, Kurschner SW, Schmid CD, Schonhaber H, Cordero J, et al. Endothelial GATA4 controls liver fibrosis and regeneration by preventing a pathogenic switch in angiocrine signaling. *J Hepatol.* 2021;74(2):380-93.
6. Semela D, Das A, Langer D, Kang N, Leof E, and Shah V. Platelet-derived growth factor signaling through ephrin-b2 regulates hepatic vascular structure and function. *Gastroenterology.* 2008;135(2):671-9.
7. Géraud C, Koch PS, Zierow J, Klapproth K, Busch K, Olsavszky V, et al. GATA4-dependent organ-specific endothelial differentiation controls liver

development and embryonic hematopoiesis. *J Clin Invest.* 2017;127(3):1099-114.

8. Mehta G, Gustot T, Mookerjee RP, Garcia-Pagan JC, Fallon MB, Shah VH, et al. Inflammation and portal hypertension - the undiscovered country. *J Hepatol.* 2014;61(1):155-63.

9. Hammoutene A, Biquard L, Lasselin J, Kheloufi M, Tanguy M, Vion AC, et al. A defect in endothelial autophagy occurs in patients with non-alcoholic steatohepatitis and promotes inflammation and fibrosis. *J Hepatol.* 2020;72(3):528-38.

10. Cao S, Liu M, Sehrawat TS, and Shah VH. Regulation and functional roles of chemokines in liver diseases. *Nat Rev Gastroenterol Hepatol.* 2021;18(9):630-47.

11. Furuta K, Guo Q, Pavelko KD, Lee JH, Robertson KD, Nakao Y, et al. Lipid-induced endothelial vascular cell adhesion molecule 1 promotes nonalcoholic steatohepatitis pathogenesis. *J Clin Invest.* 2021;131(6).

12. Gao J, Wei B, Liu M, Hirsova P, Sehrawat TS, Cao S, et al. Endothelial p300 Promotes Portal Hypertension and Hepatic Fibrosis Through C-C Motif Chemokine Ligand 2-Mediated Angiocrine Signaling. *Hepatology.* 2021;73(6):2468-83.

13. Hilscher MB, Sehrawat T, Arab JP, Zeng Z, Gao J, Liu M, et al. Mechanical stretch increases expression of CXCL1 in liver sinusoidal endothelial cells to

recruit neutrophils, generate sinusoidal microthombi, and promote portal hypertension. *Gastroenterology.* 2019;157(1):193-209.

14. Liu M, Cao S, He L, Gao J, Arab JP, Cui H, et al. Super enhancer regulation of cytokine-induced chemokine production in alcoholic hepatitis. *Nat Commun.* 2021;12(1):4560.

15. Jagavelu K, Routray C, Shergill U, O'Hara SP, Faubion W, and Shah VH. Endothelial cell toll-like receptor 4 regulates fibrosis-associated angiogenesis in the liver. *Hepatology.* 2010;52(2):590-601.

16. Thabut D, and Shah V. Intrahepatic angiogenesis and sinusoidal remodeling in chronic liver disease: new targets for the treatment of portal hypertension? *J Hepatol.* 2010;53(5):976-80.

17. Millán-Zambrano G, Burton A, Bannister AJ, and Schneider R. Histone post-translational modifications - cause and consequence of genome function. *Nat Rev Genet.* 2022;23(9):563-80.

18. Habash NW, Sehrawat TS, Shah VH, and Cao S. Epigenetics of alcohol-related liver diseases. *JHEP Rep.* 2022;4(5):100466.

19. Chemello F, Bassel-Duby R, and Olson EN. Correction of muscular dystrophies by CRISPR gene editing. *J Clin Invest.* 2020;130(6):2766-76.

20. Pankowicz FP, Jarrett KE, Lagor WR, and Bissig KD. CRISPR/Cas9: at the cutting edge of hepatology. *Gut.* 2017;66(7):1329-40.

21. Thakore PI, D'Ippolito AM, Song L, Safi A, Shivakumar NK, Kabadi AM, et al. Highly specific epigenome editing by CRISPR-Cas9 repressors for silencing of distal regulatory elements. *Nat Methods.* 2015;12(12):1143-9.

22. Gemberling MP, Siklenka K, Rodriguez E, Tonn-Eisinger KR, Barrera A, Liu F, et al. Transgenic mice for in vivo epigenome editing with CRISPR-based systems. *Nat Methods.* 2021;18(8):965-74.

23. Elwir S, Hal H, Veith J, Schreibman I, Kadry Z, and Riley T. Radiographical findings in patients with liver cirrhosis and hepatic encephalopathy. *Gastroenterol Rep (Oxf).* 2016;4(3):221-5.

24. Naylor RW, Morais M, and Lennon R. Complexities of the glomerular basement membrane. *Nat Rev Nephrol.* 2021;17(2):112-27.

25. Kisseleva T, and Brenner D. Molecular and cellular mechanisms of liver fibrosis and its regression. *Nat Rev Gastroenterol Hepatol.* 2021;18(3):151-66.

26. Tsuchida T, and Friedman SL. Mechanisms of hepatic stellate cell activation. *Nat Rev Gastroenterol Hepatol.* 2017;14(7):397-411.

27. Yaqoob U, Cao S, Shergill U, Jagavelu K, Geng Z, Yin M, et al. Neuropilin-1 stimulates tumor growth by increasing fibronectin fibril assembly in the tumor microenvironment. *Cancer Res.* 2012;72(16):4047-59.

28. Terkelsen MK, Bendixen SM, Hansen D, Scott EAH, Moeller AF, Nielsen R, et al. Transcriptional Dynamics of Hepatic Sinusoid-Associated Cells After Liver Injury. *Hepatology.* 2020;72(6):2119-33.

29. Poisson J, Lemoinne S, Boulanger C, Durand F, Moreau R, Valla D, et al. Liver sinusoidal endothelial cells: physiology and role in liver diseases. *J Hepatol.* 2017;66(1):212-27.

30. Reynaert H, Thompson MG, Thomas T, and Geerts A. Hepatic stellate cells: role in microcirculation and pathophysiology of portal hypertension. *Gut.* 2002;50(4):571-81.

31. Single-cell transcriptomics of 20 mouse organs creates a Tabula Muris. *Nature.* 2018;562(7727):367-72.

32. Xiong X, Kuang H, Ansari S, Liu T, Gong J, Wang S, et al. Landscape of Intercellular Crosstalk in Healthy and NASH Liver Revealed by Single-Cell Secretome Gene Analysis. *Mol Cell.* 2019;75(3):644-60.e5.

33. Higashijima Y, Matsui Y, Shimamura T, Nakaki R, Nagai N, Tsutsumi S, et al. Coordinated demethylation of H3K9 and H3K27 is required for rapid inflammatory responses of endothelial cells. *Embo j.* 2020;39(7):e103949.

34. Chen H, Levo M, Barinov L, Fujioka M, Jaynes JB, and Gregor T. Dynamic interplay between enhancer-promoter topology and gene activity. *Nat Genet.* 2018;50(9):1296-303.

35. Bartosovic M, Kabbe M, and Castelo-Branco G. Single-cell CUT&Tag profiles histone modifications and transcription factors in complex tissues. *Nat Biotechnol.* 2021;39(7):825-35.

36. Uyehara CM, and Apostolou E. 3D enhancer-promoter interactions and multi-connected hubs: Organizational principles and functional roles. *Cell Rep.* 2023:112068.

37. Jeanne M, Jorgensen J, and Gould DB. Molecular and Genetic Analyses of Collagen Type IV Mutant Mouse Models of Spontaneous Intracerebral Hemorrhage Identify Mechanisms for Stroke Prevention. *Circulation.* 2015;131(18):1555-65.

38. Claesson-Welsh L, Dejana E, and McDonald DM. Permeability of the Endothelial Barrier: Identifying and Reconciling Controversies. *Trends Mol Med.* 2021;27(4):314-31.

39. Su T, Yang Y, Lai S, Jeong J, Jung Y, McConnell M, et al. Single-cell transcriptomics reveals zone-specific alterations of liver sinusoidal endothelial cells in cirrhosis. *Cell Mol Gastroenterol Hepatol.* 2021;11(4):1139-61.

40. Drzewiecki K, Choi J, Brancale J, Leney-Greene MA, Sari S, Dalgiç B, et al. GIMAP5 maintains liver endothelial cell homeostasis and prevents portal hypertension. *J Exp Med.* 2021;218(7).

41. Schwabl P, Payer BA, Grahovac J, Klein S, Horvatits T, Mitterhauser M, et al. Pioglitazone decreases portosystemic shunting by modulating inflammation and angiogenesis in cirrhotic and non-cirrhotic portal hypertensive rats. *J Hepatol.* 2014;60(6):1135-42.

42. Gracia-Sancho J, Marrone G, and Fernández-Iglesias A. Hepatic microcirculation and mechanisms of portal hypertension. *Nat Rev Gastroenterol Hepatol.* 2019;16(4):221-34.

43. Reidy K, Kang HM, Hostetter T, and Susztak K. Molecular mechanisms of diabetic kidney disease. *J Clin Invest.* 2014;124(6):2333-40.

44. Mak KM, and Mei R. Basement membrane type IV collagen and laminin: an overview of their biology and value as fibrosis biomarkers of liver disease. *Anat Rec (Hoboken).* 2017;300(8):1371-90.

45. Placek K, Schultze JL, and Aschenbrenner AC. Epigenetic reprogramming of immune cells in injury, repair, and resolution. *J Clin Invest.* 2019;129(8):2994-3005.

46. Kostallari E, and Shah VH. Angiocrine signaling in the hepatic sinusoids in health and disease. *Am J Physiol Gastrointest Liver Physiol.* 2016;311(2):G246-51.

47. Wu X, Shu L, Zhang Z, Li J, Zong J, Cheong LY, et al. Adipocyte Fatty Acid Binding Protein Promotes the Onset and Progression of Liver Fibrosis

via Mediating the Crosstalk between Liver Sinusoidal Endothelial Cells and Hepatic Stellate Cells. *Adv Sci (Weinh).* 2021;8(11):e2003721.

48. Deleve LD, Wang X, and Guo Y. Sinusoidal endothelial cells prevent rat stellate cell activation and promote reversion to quiescence. *Hepatology.* 2008;48(3):920-30.

49. Xie G, Wang X, Wang L, Wang L, Atkinson RD, Kanel GC, et al. Role of differentiation of liver sinusoidal endothelial cells in progression and regression of hepatic fibrosis in rats. *Gastroenterology.* 2012;142(4):918-27.

50. Fallowfield JA, Hayden AL, Snowdon VK, Aucott RL, Stutchfield BM, Mole DJ, et al. Relaxin modulates human and rat hepatic myofibroblast function and ameliorates portal hypertension in vivo. *Hepatology.* 2014;59(4):1492-504.

51. Sprangers S, and Everts V. Molecular pathways of cell-mediated degradation of fibrillar collagen. *Matrix Biol.* 2019;75-76:190-200.

52. Singh P, Carraher C, and Schwarzbauer JE. Assembly of fibronectin extracellular matrix. *Annu Rev Cell Dev Biol.* 2010;26:397-419.

53. Lu J, Doyle AD, Shinsato Y, Wang S, Bodendorfer MA, Zheng M, et al. Basement Membrane Regulates Fibronectin Organization Using Sliding Focal Adhesions Driven by a Contractile Winch. *Dev Cell.* 2020;52(5):631-46 e4.

54. Xu M, Xu HH, Lin Y, Sun X, Wang LJ, Fang ZP, et al. LECT2, a Ligand for Tie1, Plays a Crucial Role in Liver Fibrogenesis. *Cell.* 2019;178(6):1478-92 e20.

55. Yang L, Kwon J, Popov Y, Gajdos GB, Ordog T, Brekken RA, et al. Vascular endothelial growth factor promotes fibrosis resolution and repair in mice. *Gastroenterology.* 2014;146(5):1339-50.

56. Carmeliet P, and Jain RK. Molecular mechanisms and clinical applications of angiogenesis. *Nature.* 2011;473(7347):298-307.

57. Chen D, Hughes ED, Saunders TL, Wu J, Vasquez MNH, Makinen T, et al. Angiogenesis depends upon EPHB4-mediated export of collagen IV from vascular endothelial cells. *JCI Insight.* 2022;7(4).

58. Wang H, and Su Y. Collagen IV contributes to nitric oxide-induced angiogenesis of lung endothelial cells. *Am J Physiol Cell Physiol.* 2011;300(5):C979-88.

59. Greuter T, Yaqoob U, Gan C, Jalan-Sakrikar N, Kostallari E, Lu J, et al. Mechanotransduction-induced glycolysis epigenetically regulates a CXCL1-dominant angiocrine signaling program in liver sinusoidal endothelial cells in vitro and in vivo. *J Hepatol.* 2022;77(3):723-34.

60. Cao S, Yaqoob U, Das A, Shergill U, Jagavelu K, Huebert RC, et al. Neuropilin-1 promotes cirrhosis of the rodent and human liver by enhancing

PDGF/TGF-beta signaling in hepatic stellate cells. *J Clin Invest.* 2010;120(7):2379-94.

Figure 1. Collagen type IV (COL4) is increased in human and mouse fibrotic livers. (**A**) Differential gene expression analysis showed a wide array of collagen genes with increased expression (log_2-fold change [Log2FC] >2) in alcohol-induced human cirrhotic livers. Red box highlights COL4 genes. (**B**) Expression level of upregulated collagen genes in healthy and cirrhotic human livers was quantified via Integrative Genomics Viewer. Other than *COL1A1*, both *COL4A1* and *COL4A2* (blue arrows) showed the highest reads per kilobase per million mapped reads (RPKM) in cirrhotic livers. (**C**-**D**) Representative immunofluorescence (IF) images showed COL4 staining (green) and LYVE1 staining (red) in human (**C**) and mouse (**D**) livers. Besides each image is the colocalization analysis for each of the merged images. The graph peaks represent the average fluorescence intensities of the staining at the given distances (in nanometers) along the four straight white arrows in each sinusoid. The white arrows in the merged images represent the areas selected for colocalization. Each graph has number of intensity peaks for each fluorophore (green and red). The ratio of intensity peaks of COL4 vs LYVE1 is shown on the top of each graph. Total three complete sinusoids have been quantified for colocalization analysis (n=3/group). IF images showed close approximation of COL4 with Lyve1 in both in human and mouse normal and cirrhotic liver. DAPI (blue) was used to stain nuclei. COL4 expression was upregulated in liver sinusoids from alcohol-induced human cirrhotic livers (**C**) and from CCl_4-induced mouse fibrotic livers (**D**). Graphs represent mean ± SEM. **P*<.05, ***P*<.01, 2-tailed unpaired Student's *t* test.

Figure 2. Liver sinusoidal endothelial cells (LSECs) are the main source of *Col4a1* and *Col4a2* in healthy and pathologic conditions. Single-cell RNA sequencing (scRNA-Seq) analysis was performed on normal (olive oil) and fibrotic (CCl_4) mouse livers. (**A**) t-Distributed stochastic neighbor embedding (tSNE) analysis identified 17 main cell clusters (numbered) in the liver using distinct gene markers. Among them, *Lyve1* was a marker for LSECs, which represent clusters 2 and 11. Each orange dot represents an individual LSEC. Other cell clusters were also identified based on the conserved genes of each cell type. Clusters 1, 4, 9, and 13 were identified as hepatocytes, cluster 5 as HSCs, cluster 3 as Kupffer cells, clusters 10 and 12 as macrophages, cluster 16 as cholangiocytes. The rest of clusters represent other immune cells, including T cells, B cells and neutrophils. (**B**) Violin plots for scRNA-Seq data from the 17 cell clusters show that *Col4a1* and *Col4a2* were mainly expressed by LSECs, and the expressions were higher in fibrotic livers. (**C**) By analyzing percentage of cells expressing the gene, log2FC of gene in fibrotic vs healthy livers, and adjusted $P<.05$ (Adjusted P-value from DESeq2), the 3D plot showed increased *Col4a1* and *Col4a2* in LSEC clusters in mouse fibrotic livers. (**D**) By quantitative real-time polymerase chain reaction (qPCR) assays of isolated LSECs and hepatic stellate cells (HSCs) from mouse normal and fibrotic livers, LSECs, but not HSCs, from fibrotic livers showed markedly increased *Col4a1* and *Col4a2* gene expression (n=3/group). Graphs represent mean ± SEM. *$P<.05$, **$P<.01$, 2-tailed unpaired Student's *t* test.

Figure 3. Tumor necrosis factor-α (TNFα) induces expression of *COL4A1* and *COL4A2* in a nuclear factor–κB (NF-κB)-dependent manner. (**A**) qPCR assays were performed on human LSECs treated with vehicle or TNFα from 4 to 24 h. mRNA levels of *COL4A1* and *COL4A2* were highest after 12 h of TNFα treatment. *CXCL1* was a positive control (n=3, biologically independent samples). (**B**-**C**) Human LSECs were pretreated with the NF-κB inhibitor celastrol before 12 h of TNFα stimulation. Celastrol strikingly blocked the increase in *COL4A1*, *COL4A2*, and *CXCL1* mRNA levels (**B**) and COL4 protein (**C**) induced by TNFα stimulation (n=3-4, biologically independent samples). Green indicates COL4 stained with anti-COL4 antibody; red, phalloidin staining of actin filaments; blue, DAPI staining of DNA; white arrows, secreted COL4 protein. Graphs represent mean ± SEM. *$P<.05$, **$P<.01$, ***$P<.001$, 1-way ANOVA followed by Bonferroni's post-test.

Figure 4. Epigenetic repression of the enhancer-promoter interaction silences *Col4a1* and *Col4a2* gene expression in response to TNFα stimulation. Isolated LSECs from *dCas9-KRAB/Cdh5*$^{\mathrm{CreERT2}}$ mice after in vivo tamoxifen injection were transfected with single-guide RNAs (sgRNAs), which target the bi-directional promoter region or putative enhancer regions of the COL4 genes. Non-targeting sgRNA was used as a negative control. (**A**) Among sgRNAs targeting the bi-directional promoter region, sgRNAs 4 (sg4) and 5 (sg5) most strongly repressed the expression of *Col4a1* and *Col4a2* (red boxes) compared with non-targeting sgRNA via qPCR assay (n=3, biologically independent samples). (**B**) Among sgRNAs targeting the putative enhancer regions, sgER1-1 (red boxes) most strongly repressed the expression of *Col4a1* and *Col4a2* compared with non-targeting sgRNA via qPCR (n=4, biologically independent samples). (**C**) Chromatin immunoprecipitation (ChIP)-qPCR assay revealed decreased H3K4me3 enrichment at the promoter region, as well as decreased H3K27ac enrichment at the putative enhancer region, after sg4 and sg5 transfection into isolated mouse LSECs expressing dCas9-KRAB (n=3, biologically independent samples). (**D**) ChIP-qPCR showed decreased H3K27ac enrichment at the putative enhancer region, as well as decreased H3K4me3 enrichment at the promoter region, after sgER1-1 was transfected into isolated mouse LSECs expressing dCas9-KRAB (n=3, biologically independent samples). (**E**) ChIP-qPCR showed increased H3K9me3 enrichment at the corresponding region when sgRNAs targeted the promoter or putative enhancer regions (n=3, biologically independent samples). Graphs represent mean ± SEM. *$P<.05$, **$P<.01$, ***$P<.001$, 1-way ANOVA followed by Bonferroni's post-test.

Figure 5. LSEC-specific COL4 contributes to portal hypertension (PHTN). (**A**) LSEC-specific *Col4a1* mutant mice were generated by crossing *Col4a1*$^{fl/wt}$ mice with *Cdh5*^{CreERT2} mice. *Col4a1* mutation was induced by deleting exon 41 to produce a truncated dysfunctional COL4 protein. LSECs were isolated from *Col4a1*$^{fl/wt}$ and *Col4a1*$^{fl/wt}$/*Cdh5*^{CreERT2} mice after in vivo tamoxifen administration to extract DNA for PCR. Post-PCR gel showed a lower-molecular-weight band after Cre recombinase treatment to excise the floxed exon 41 sequence in *Col4a1*$^{fl/wt}$/*Cdh5*^{CreERT2} mouse LSECs (red arrow). (**B**) COL4 immunogold staining of mouse liver tissues showed that COL4 protein was secreted and deposited in liver sinusoids from *Col4a1*$^{fl/wt}$ mice (red arrow), whereas LSEC-specific *Col4a1* mutation inhibited COL4 deposition. Bottom images are magnifications of red boxes on top images. (**C**) To induce PHTN, *Col4a1*$^{fl/wt}$ and *Col4a1*$^{fl/wt}$/*Cdh5*^{CreERT2} mice were subjected to 6 weeks of CCl_4 administration (or olive oil for control). CCl_4 injection increased portal pressure by 2-fold in *Col4a1*$^{fl/wt}$ mice, whereas this increase was abrogated by *Col4a1* mutation in LSECs (n=8-13/group). (**D**) The ratio of spleen weight to body weight was increased after CCl_4 administration, which was blocked by LSEC *Col4a1* mutation (n=7-10/group). (**E**) To explore liver sinusoidal permeability, 4-kDa FITC-dextran was administered via the tail vein. It passed through LSECs and was endocytosed by hepatocytes (red stars) in healthy livers. In contrast, FITC-dextran failed to cross the membrane of CCl_4-induced LSECs, gathering at the sinusoidal line (red arrows). FITC-dextran was noticeable in hepatocytes from *Col4a1*-mutated livers even with CCl_4 treatment, which indicates that COL4 blocks sinusoidal permeability (n=4/group). Graphs represent mean ± SEM. **P*<.05, ***P*<.01, 1-way ANOVA followed by Bonferroni's post-test.

Figure 6. LSEC-specific COL4 promotes sinusoidal resistance. (**A**) After PHTN model establishment, LSECs were isolated for qPCR analysis. Results showed increased expression of *Cd34* (capillarization marker) and decreased expression of *Lyve1* and *Stab1* (LSEC markers) in CCl_4-induced LSECs. In contrast, *Col4a1* mutation in LSECs maintained the LSEC phenotype, as shown by a decrease in *Cd34* and an increase in *Lyve1* and *Stab1* levels (n=3/group). Graphs represent mean ± SEM. **P*<.05, ***P*<.01, ****P*<.001, 1-way ANOVA followed by Bonferroni's post-test. (**B**-**C**) Healthy LSECs had characteristic fenestrae (red arrows) on transmission electron microscopy (TEM) (**B**) and a sieve plate (red stars) on scanning electron microscopy. (**C**). Bottom images in B are magnifications of red boxes on top images. In contrast, CCl_4 induced the defenestration of LSECs, indicated by the loss of fenestrae and formation of basement membrane (black arrows), as well as other collagens deposition in perisinusoidal space (black star). *Col4a1* mutation in LSECs restored the LSEC phenotype by maintaining the fenestrae and sieve plate. (n=2/group for TEM and SEM).

Figure 7. COL4 serves as a scaffold for COL1 deposition and assembly in liver sinusoids to contribute to sinusoidal resistance and stiffness. (**A**) Representative immunohistochemical (IHC) staining of mouse liver tissues showed a significant decrease in COL1 deposition in liver sinusoids from *Col4a1*$^{fl/wt}$/*Cdh5*^{CreERT2} mice compared with *Col4a1*$^{fl/wt}$ mice that had CCl_4 administration (n=5/group). (**B**) 3D high-resolution images of liver tissues were obtained and reconstructed to show the location of COL1 (red) and COL4 (green) in liver sinusoids (DAPI, blue, indicates the nucleus). The overlapping collagens (yellow) showed that the bulk of the COL1 was surrounded and supported by COL4 in CCl_4-administered mouse livers. In contrast, COL4 deposition in liver sinusoid was abrogated by *Col4a1* mutation in LSECs. The lack of COL4 scaffold induced patchy and discontinuous COL1 deposition in liver sinusoids (n=3/group). Graphs represent mean ± SEM. *P<.05, **P<.01, 2-tailed unpaired Student's *t* test.

Figure 8. COL4 contributes to sinusoidal remodeling via activating angiogenic sprouting of LSECs. (**A**) Representative IF images of isolated LSECs stained for Col4a1 (red) and Hsp47 (green) (DAPI, blue, indicates nucleus.) Mice with PHTN showed Col4a1 production and secretion in LSECs (white arrows), whereas *Col4a1* mutation in LSECs led to dysfunctional Col4a1 retained in endoplasmic reticulum (ER, red arrows). Hsp47 is a chaperone located in ER to help collagen synthesis. Images in the first column are magnifications of white boxes in the second column (n=3/group). (**B-C**) Human LSECs were transfected with *COL4A1* small interfering RNA (siRNA) to knock down the expression of COL4. *Scramble* siRNA was used as a negative control. (**B**) qPCR results showed decreased COL4 expression in human LSECs after *COL4A1* siRNA transfection. (**C**) *COL4A1* siRNA-transfected human LSECs were plated in 3D fibrin gel and treated with TNFα. Representative IF images of fibrin gel stained for COL4 (green) showed it to be secreted extracellularly and organized into COL4 bundles and tubules. These formed tubes in the *scramble* siRNA group, shown by increased branch points, but *COL4A1* knockdown inhibited tube formation due to the lack of COL4 production and secretion (n=3, biologically independent samples). Green indicates COL4 stained with anti-COL4 antibody; red, phalloidin staining of actin filaments; blue, DAPI staining of DNA. Graphs represent mean ± SEM. *$P<.05$, ***$P<.001$, 2-tailed unpaired Student's *t* test.

Figure 9. Epigenetic repression of LSEC-derived COL4 alleviates PHTN. (**A**) Schematic of *dCas9-KRAB/Cdh5*^{CreERT2} mice undergoing tamoxifen injection, adeno-associated virus (AAV) delivery, and PHTN establishment. (**B**) CCl_4 administration increased portal pressure by 70% in mice with control AAV (AAV-non) delivery, whereas this increase was abrogated by 25% to 30% in mice with AAV-sg4 or AAV-sg5 (n=5-6/group). (**C**) Representative IF staining showed that increased COL4 expression in liver sinusoids after CCl_4 injection was blocked in mice treated with AAV-sg4 or AAV-sg5 (n=5/group). (**D**) Representative IHC staining of liver tissues showed a significant increase in sinusoidal Cd34 level in mice that underwent CCl_4 administration and were treated with control AAV vs with AAV-sg4 or AAV-sg5 (n=5/group). (**E**-**F**) After 6 weeks of CCl_4 administration, LSECs were isolated for qPCR analysis. Decreased expression of *Col4a1* and *Col4a2* (**E**), as well as decreased expression of *Cd34* (**F**), were noted in mice with AAV-sg4 or AAV-sg5 delivery (n=3/group). Graphs represent mean ± SEM. *P<.05, **P<.01, ***P<.001, 1-way ANOVA followed by Bonferroni's post-test.

Figure 1

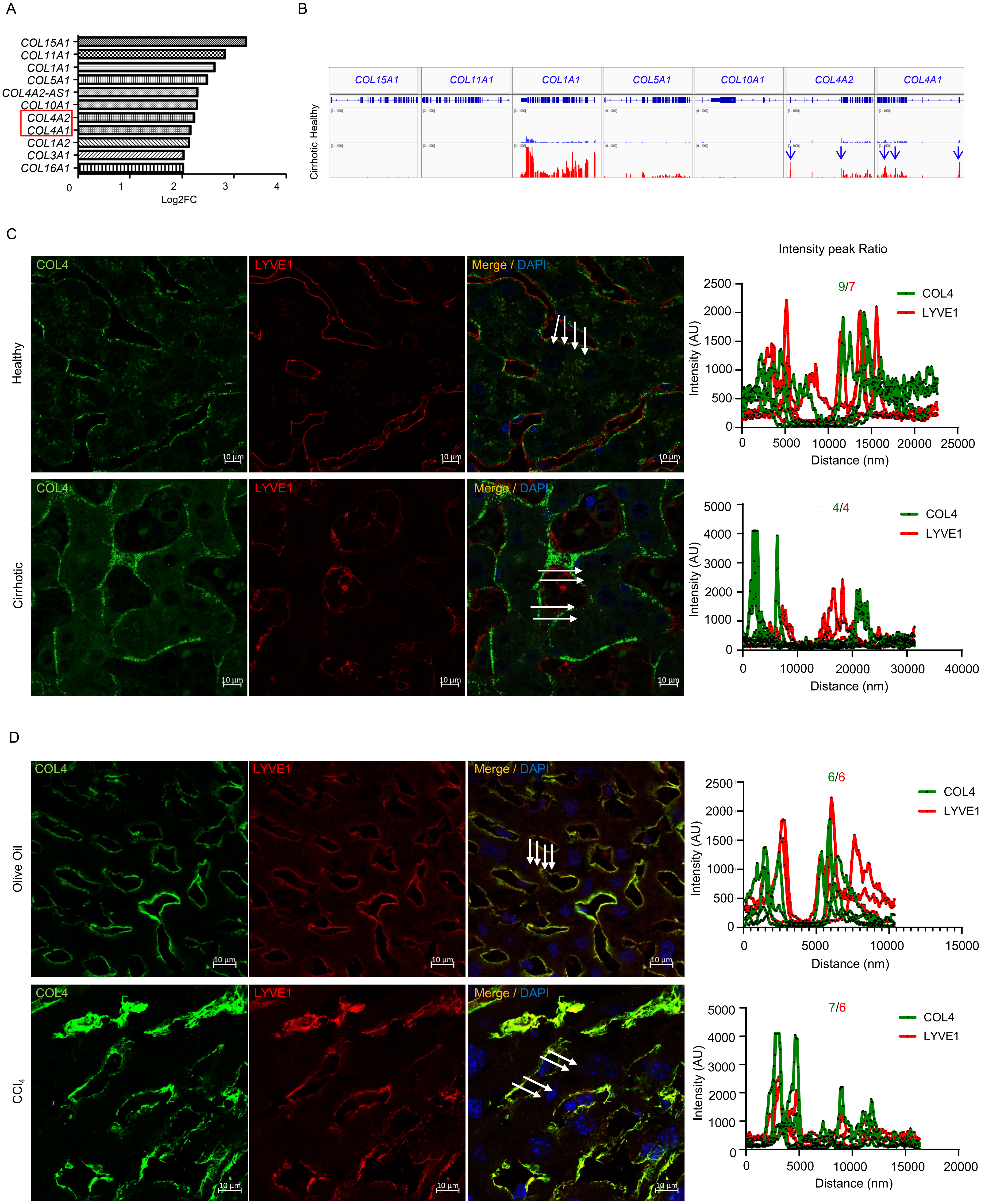

A
COL15A1
COL11A1
COL1A1
COL5A1
COL4A2-AS1
COL10A1
COL4A2
COL4A1
COL1A2
COL3A1
COL16A1
0
1
2
3
4
Log2FC
B
COL15A1
COL11A1
COL1A1
COL5A1
COL10A1
COL4A2
COL4A1
Healthy
Cirrhotic
C
Intensity peak Ratio
Healthy
Cirrhotic
COL4
LYVE1
Merge / DAPI
10 µm
9/7
4/4
Intensity (AU)
Distance (nm)
D
Olive Oil
CCl4
6/6
7/6

Figure 2

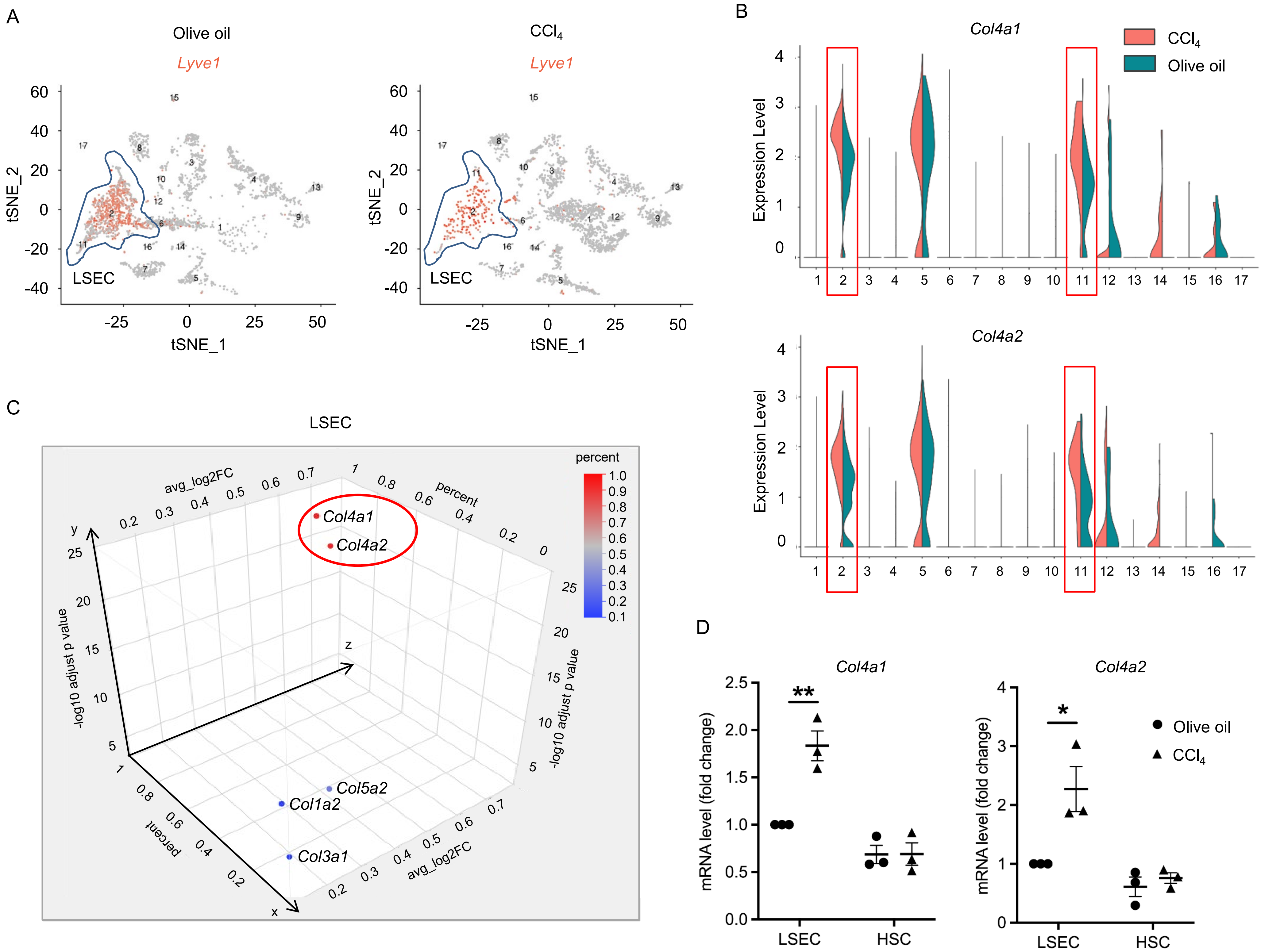
A
Olive oil
Lyve1
CCl4
Lyve1
tSNE_2
tSNE_1
LSEC
B
Col4a1
Col4a2
CCl4
Olive oil
Expression Level
C
LSEC
avg_log2FC
percent
-log10 adjust p value
Col4a1
Col4a2
Col5a2
Col1a2
Col3a1
D
Col4a1
Col4a2
mRNA level (fold change)
Olive oil
CCl4
LSEC
HSC

Figure 3

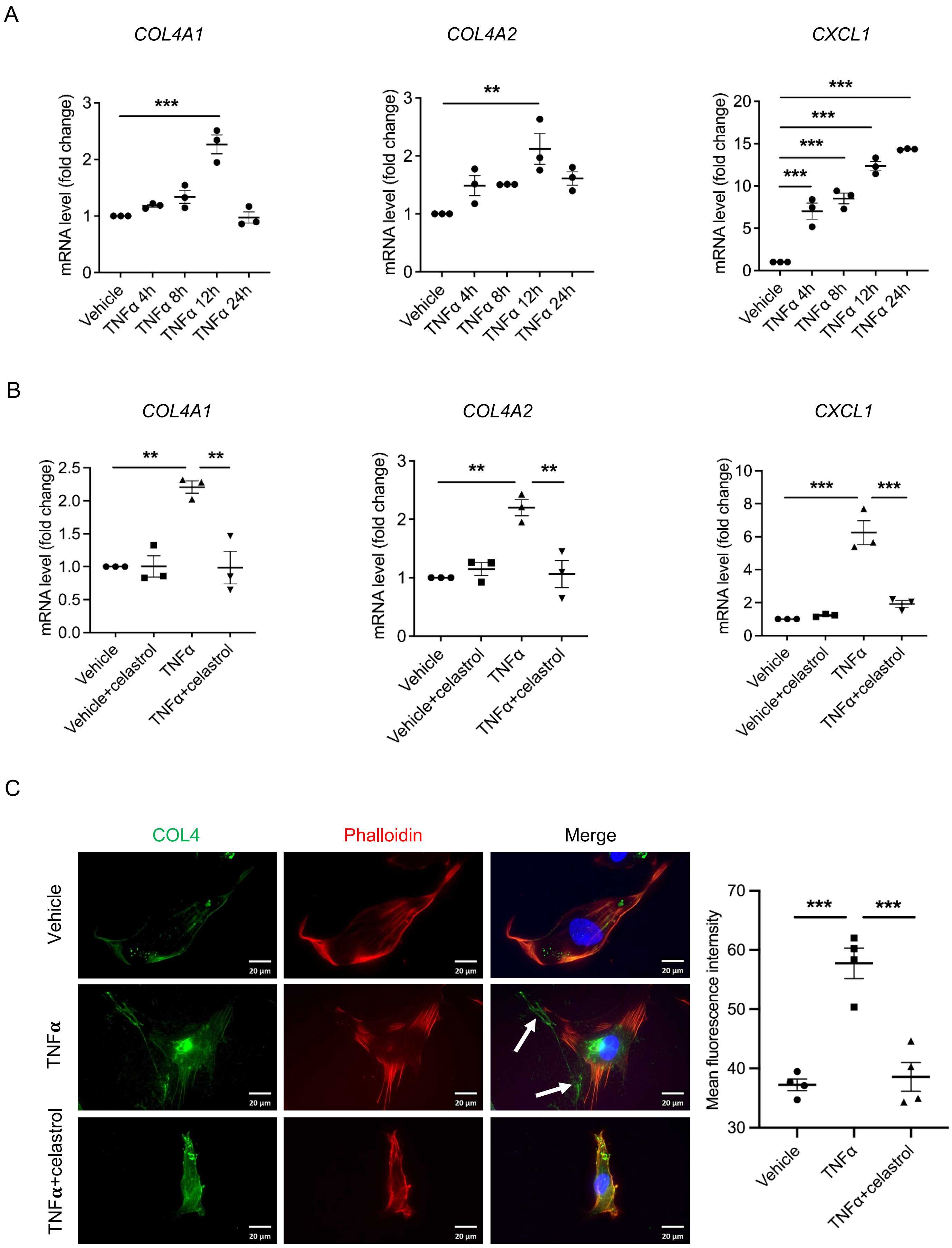
A
COL4A1
COL4A2
CXCL1
mRNA level (fold change)
Vehicle
TNFα 4h
TNFα 8h
TNFα 12h
TNFα 24h
B
COL4A1
COL4A2
CXCL1
mRNA level (fold change)
Vehicle
Vehicle+celastrol
TNFα
TNFα+celastrol
C
COL4
Phalloidin
Merge
Vehicle
TNFα
TNFα+celastrol
20 μm
Mean fluorescence intensity

Figure 4

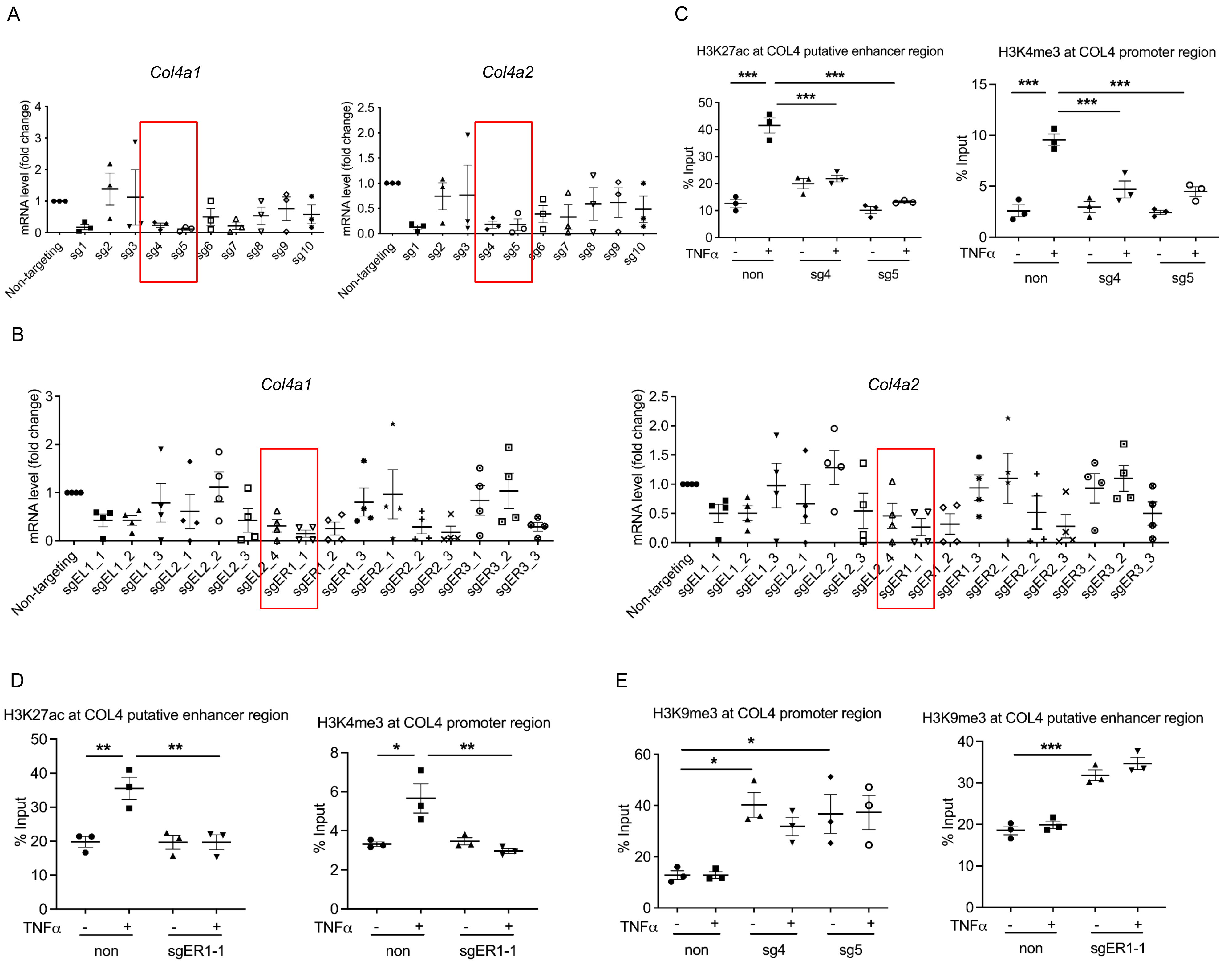
A
Col4a1
Col4a2
mRNA level (fold change)
Non-targeting
sg1
sg2
sg3
sg4
sg5
sg6
sg7
sg8
sg9
sg10
B
Col4a1
Col4a2
mRNA level (fold change)
Non-targeting
sgEL1_1
sgEL1_2
sgEL1_3
sgEL2_1
sgEL2_2
sgEL2_3
sgEL2_4
sgER1_1
sgER1_2
sgER1_3
sgER2_1
sgER2_2
sgER2_3
sgER3_1
sgER3_2
sgER3_3
C
H3K27ac at COL4 putative enhancer region
H3K4me3 at COL4 promoter region
% Input
TNFα
non
sg4
sg5
D
H3K27ac at COL4 putative enhancer region
H3K4me3 at COL4 promoter region
% Input
TNFα
non
sgER1-1
E
H3K9me3 at COL4 promoter region
H3K9me3 at COL4 putative enhancer region
% Input
TNFα
non
sg4
sg5
sgER1-1

Figure 5

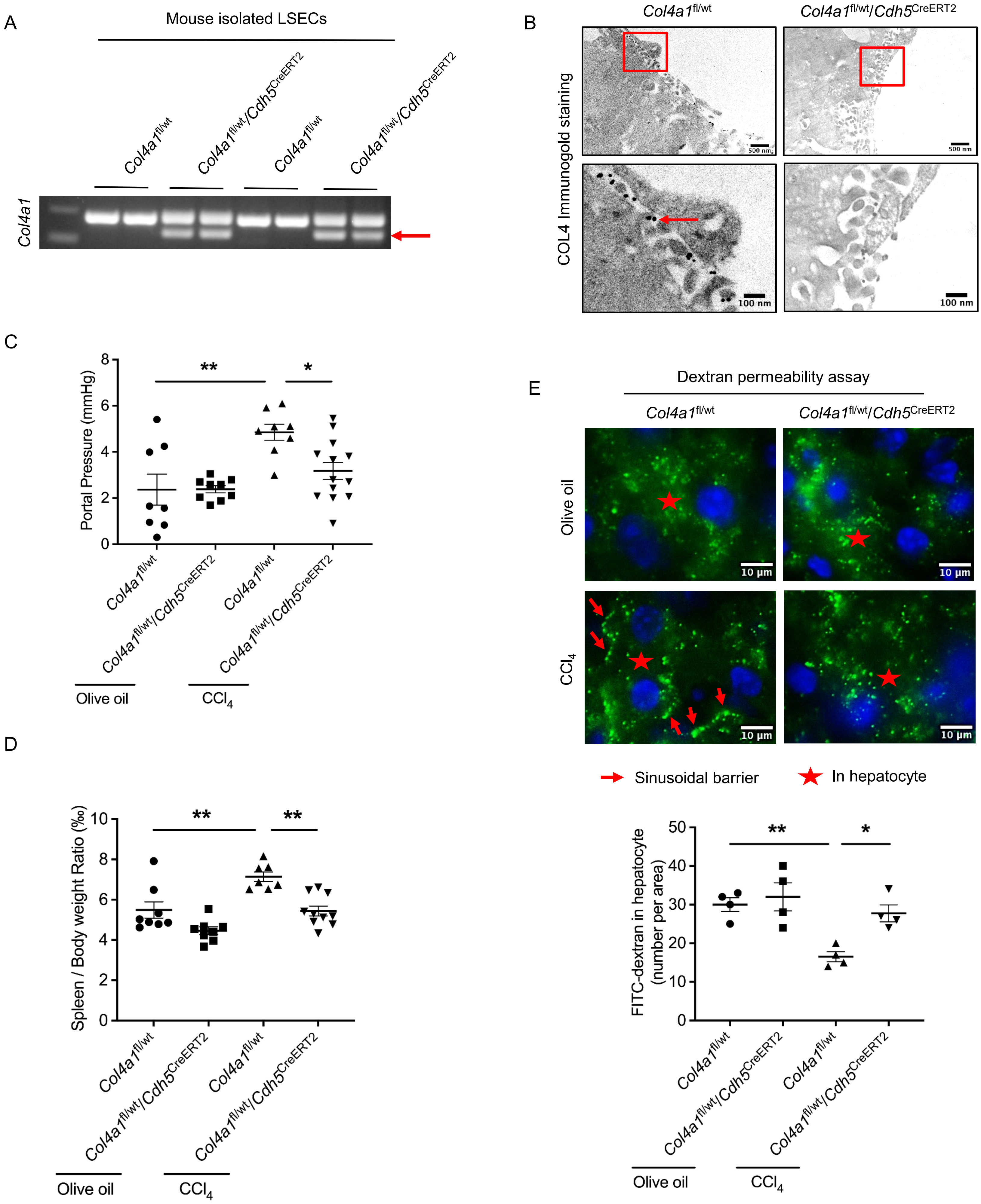

A
Mouse isolated LSECs
Col4a1fl/wt
Col4a1fl/wt/Cdh5CreERT2
Col4a1fl/wt
Col4a1fl/wt/Cdh5CreERT2
Col4a1
B
Col4a1fl/wt
Col4a1fl/wt/Cdh5CreERT2
COL4 Immunogold staining
500 nm
100 nm
C
Portal Pressure (mmHg)
Olive oil
CCl4
D
Spleen / Body weight Ratio (‰)
Olive oil
CCl4
E
Dextran permeability assay
Col4a1fl/wt
Col4a1fl/wt/Cdh5CreERT2
Olive oil
CCl4
10 μm
Sinusoidal barrier
In hepatocyte
FITC-dextran in hepatocyte (number per area)
Olive oil
CCl4

Figure 6

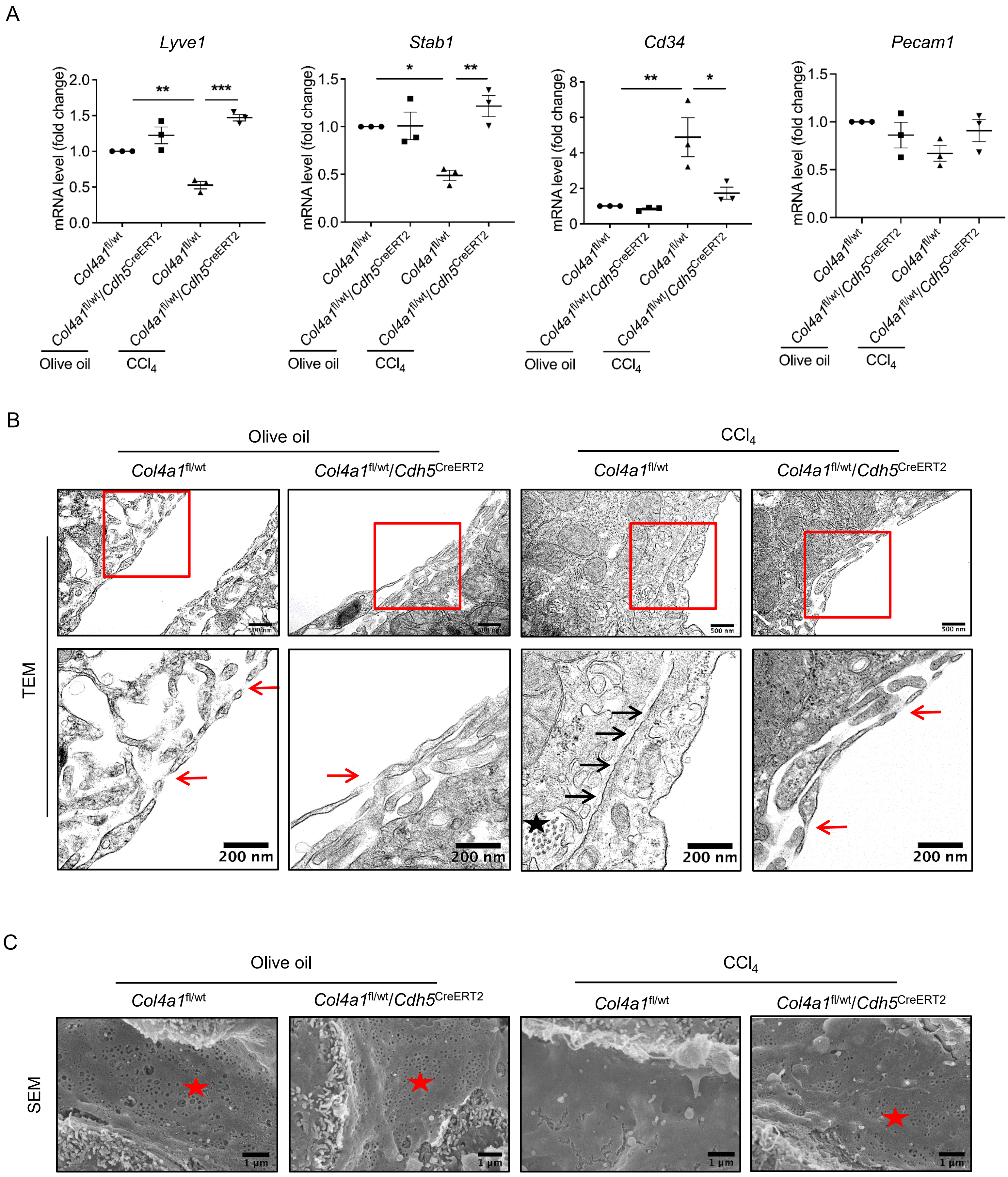

A
Lyve1
Stab1
Cd34
Pecam1
mRNA level (fold change)
**
***
*
Col4a1fl/wt
Col4a1fl/wt/Cdh5CreERT2
Olive oil
CCl4
B
TEM
200 nm
C
SEM
1 μm

Figure 7

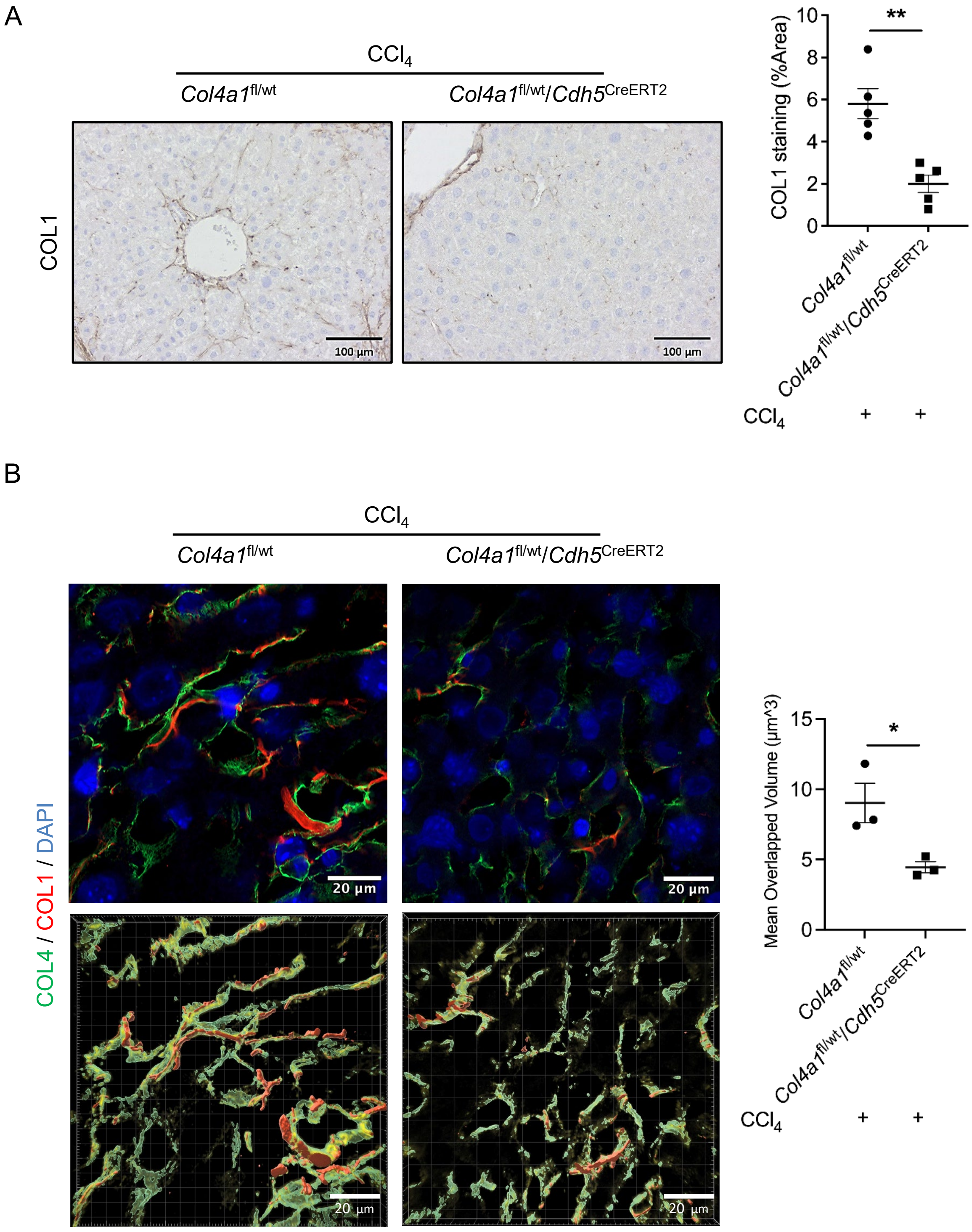

A
CCl4
Col4a1fl/wt
Col4a1fl/wt/Cdh5CreERT2
COL1
100 µm
100 µm
COL1 staining (%Area)
**
Col4a1fl/wt
Col4a1fl/wt/Cdh5CreERT2
CCl4 + +
B
CCl4
Col4a1fl/wt
Col4a1fl/wt/Cdh5CreERT2
COL4 / COL1 / DAPI
20 µm
Mean Overlapped Volume (µm^3)
*
Col4a1fl/wt
Col4a1fl/wt/Cdh5CreERT2
CCl4 + +

Figure 8

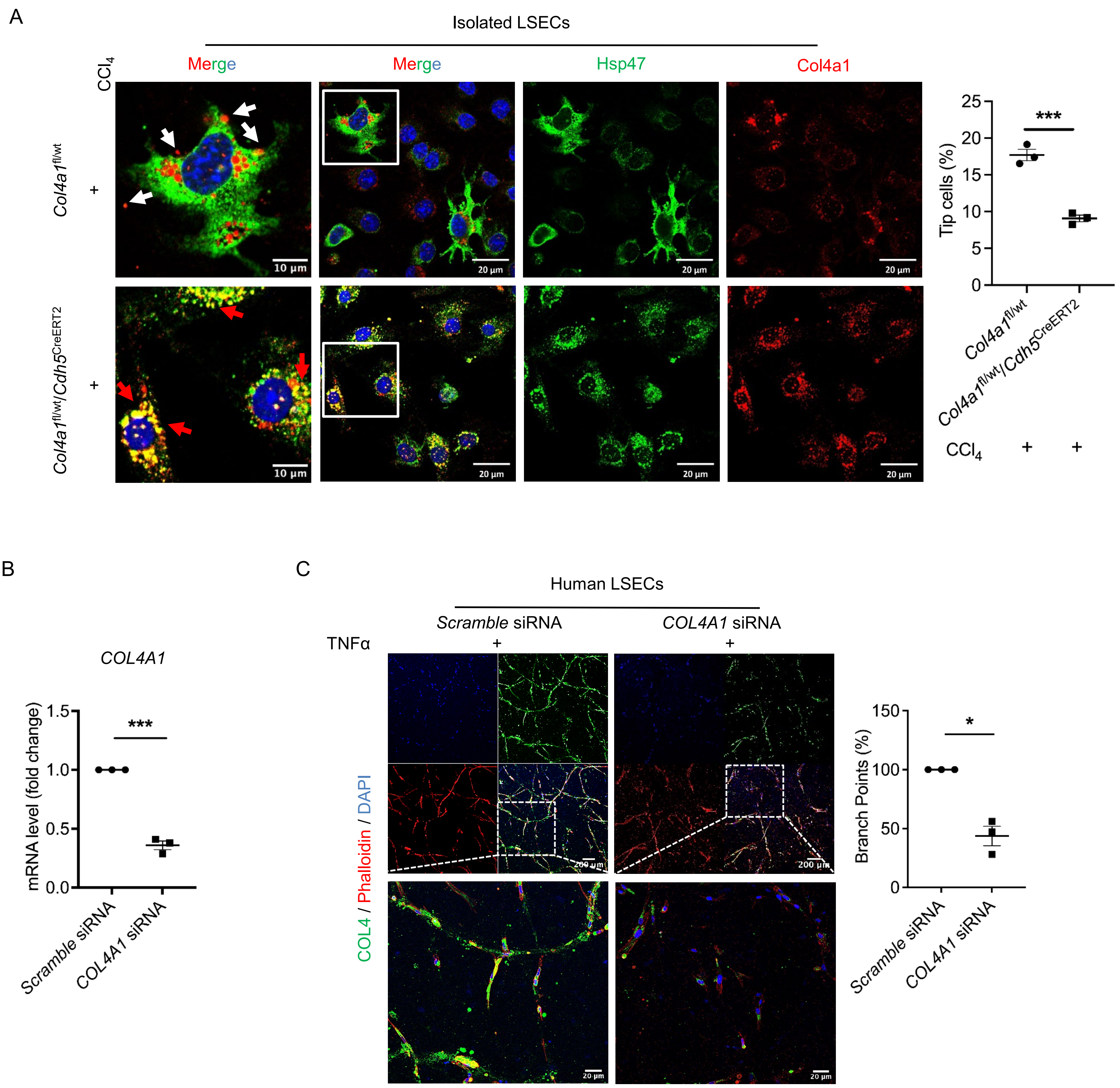

A
Isolated LSECs
CCl4
Merge
Merge
Hsp47
Col4a1
Col4a1fl/wt
+
Col4a1fl/wt/Cdh5CreERT2
+
10 µm
20 µm
25
20
15
10
5
0
Tip cells (%)
***
Col4a1fl/wt
Col4a1fl/wt/Cdh5CreERT2
CCl4
+
+
B
COL4A1
1.5
1.0
0.5
0.0
mRNA level (fold change)
***
Scramble siRNA
COL4A1 siRNA
C
Human LSECs
Scramble siRNA
COL4A1 siRNA
TNFα
+
+
COL4 / Phalloidin / DAPI
200 µm
20 µm
150
100
50
0
Branch Points (%)
*
Scramble siRNA
COL4A1 siRNA

Figure 9

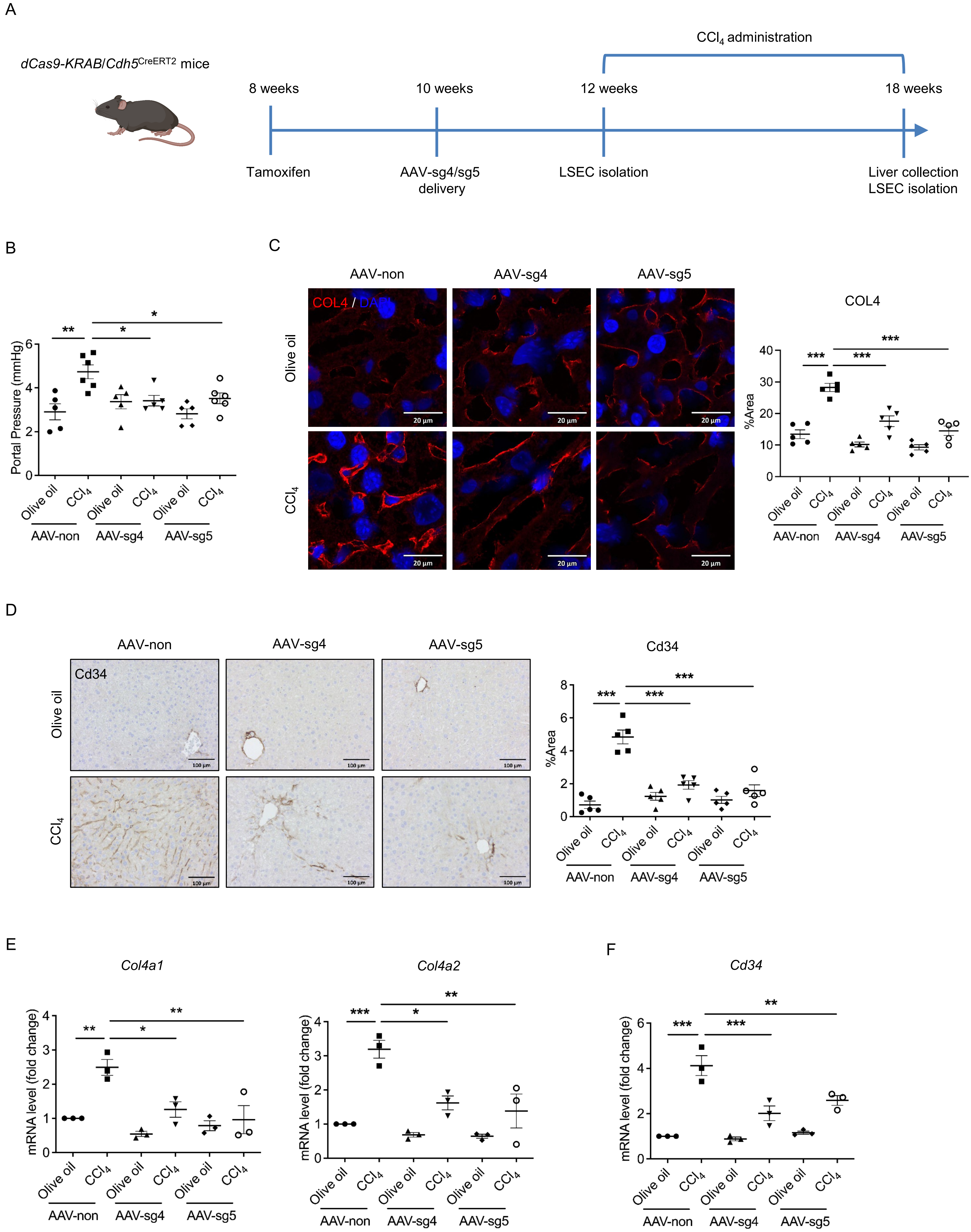
A
dCas9-KRAB/Cdh5CreERT2 mice
CCl4 administration
8 weeks
10 weeks
12 weeks
18 weeks
Tamoxifen
AAV-sg4/sg5 delivery
LSEC isolation
Liver collection
LSEC isolation
B
Portal Pressure (mmHg)
Olive oil
CCl4
AAV-non
AAV-sg4
AAV-sg5
C
AAV-non
AAV-sg4
AAV-sg5
COL4 / DAPI
Olive oil
CCl4
COL4
%Area
D
AAV-non
AAV-sg4
AAV-sg5
Cd34
Olive oil
CCl4
%Area
E
Col4a1
Col4a2
mRNA level (fold change)
F
Cd34
mRNA level (fold change)